Tunable Wettability of a Dual-Faced Covalent Organic Framework Membrane for Enhanced Water Filtration

Farah Benyettou, Asmaa Jrad, Zineb Matouk, Thirumurugan Prakasam, Houeida Issa Hamoud, Guillaume Clet, Sabu Varghese, Gobinda Das, Mostafa Khair, Sudhir Kumar Sharma, et al.

Tunable Wettability of a Dual-Faced COF Membrane for Enhanced Water Filtration

*Farah Benyettou,[†*1] Asmaa Jrad,[†,1,2] Zineb Matouk,[3] Thirumurugan Prakasam,[1] Houeida Issa Hamoud,[4] Guillaume Clet,[4] Sabu Varghese,[5] Gobinda Das,[1] Mostafa Khair,[5] Sudhir Kumar Sharma,[1] Bikash Garai,[1,2] Rasha G. AbdulHalim,[1] Maryam Alkaabi,[1] Jamaliah Aburabie,[1,2] Sneha Thomas,[5] James Weston,[5] Renu Pasricha,[5] Ramesh Jagannathan,[1] Felipe Gándara,[6] Mohamad El-Roz,[4] Ali Trabolsi**[1,2]*

† equal contribution

1. Chemistry Program, New York University Abu Dhabi (NYUAD), P.O. Box 129188, Abu Dhabi, United Arab Emirates.
2. NYUAD Water Research Center, New York University Abu Dhabi (NYUAD), Saadiyat Island, Abu Dhabi, United Arab Emirates
3. Technology Innovative Institute, P.O. Box 9639, Abu Dhabi, United Arab Emirates.
4. Normandie Univ, ENSICAEN, UNICAEN, CNRS, LCS, 14000 Caen, France.
5. Core Technologies Platform, New York University Abu Dhabi, 129188, Abu Dhabi, United Arab Emirates.
6. Instituto de Ciencia de Materiales de Madrid-CSIC, C. Sor Juana Inés de la Cruz 3, 28049 Madrid, Spain

**Correspondence: fb51@nyu.edu*
***Correspondence: at105@nyu.edu*

Graphical abstract

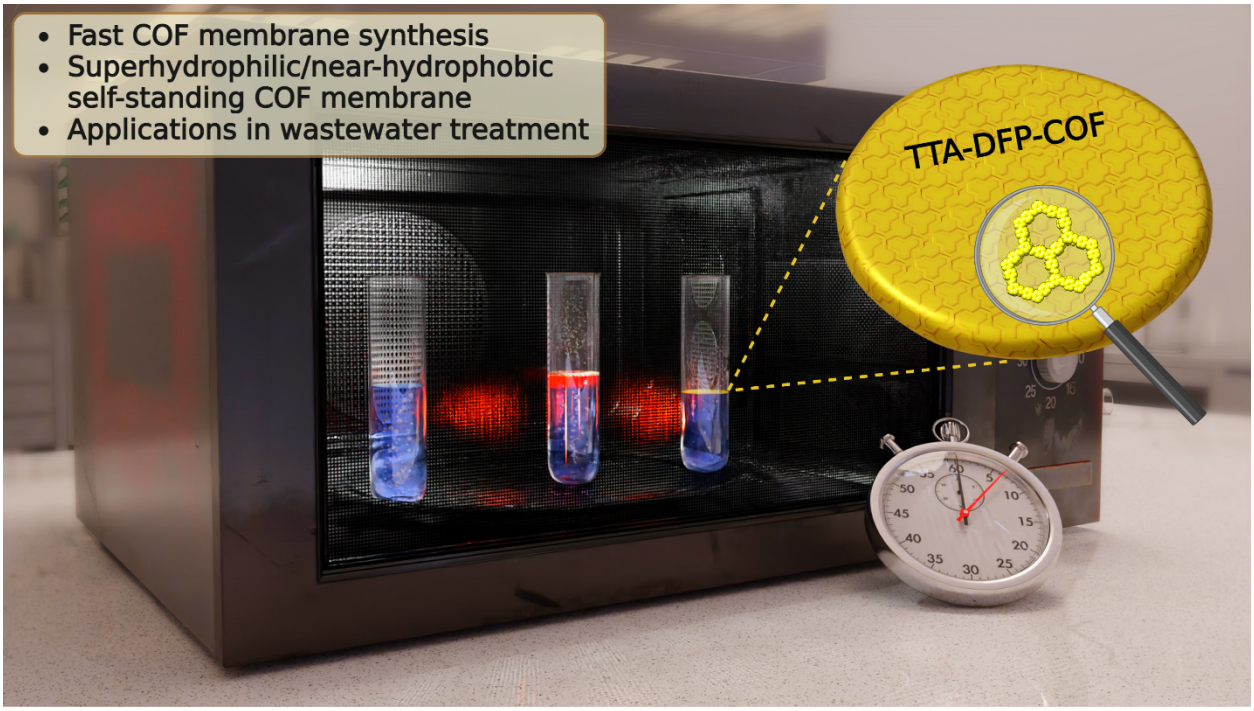

The bigger picture

The global quest for sustainable and efficient water treatment technologies requires innovation in membrane design and functionality. Traditional membrane technologies, while effective, can be energy-intensive and may lack specificity or longevity. This signifies the dawn of a new period in networked materials, with a specific focus on Covalent Organic Frameworks (COFs). These materials, known for their precise tunability and self-assembling properties, promise advances in water purification, gas adsorption, energy storage, and more. However, a major challenge lies in the time-consuming synthesis of COFs and in effectively modifying their surface properties.

This study presents a breakthrough approach for the synthesis of COF membranes by a microwave-mediated interfacial polymerization method. This technique not only dramatically shortens the synthesis time but also provides unprecedented control over the surface properties of the membranes, allowing one side to be superhydrophilic and the other to be nearly hydrophobic. Such dual properties in one membrane are groundbreaking. The synthesized TTA-DFP-COF membrane features improved water permeability, resistance to organic fouling, and remarkable oil separation capacity.

The real-world implications of this research are enormous. The rapid and efficient synthesis of TTA-DFP-COF membranes, combined with their remarkable separation and anti-fouling capabilities, positions this technology as a frontrunner for future water treatment solutions in the face of growing global water challenges. It represents not only an advance in membrane technology but also a significant step towards addressing pressing environmental issues.

Summary

Membrane technology is pivotal for advancing separation processes, notably in water treatment. This realm sees transformative potential with Covalent Organic Frameworks (COFs), praised for their adjustable structures and robustness. However, conventional COF membrane synthesis methods often face challenges, such as time-consuming processes and limited control over surface properties. Our study unveils a groundbreaking, swift, microwave-assisted method of synthesizing self-standing COF membranes within minutes. This approach masters surface property manipulation, achieving superhydrophilic and near-hydrophobic characteristics. State-of-the-art analyses validate the membrane's integrity and wetting property mastery. Microwave activation expedites COF nanosheets' self-assembly, with adjustable reaction times dictating membrane thickness. Unique in composition, the membrane's superhydrophilic vapor side results from -NH_2 reactions with acetic acid, and the nearly-hydrophobic dioxane side features terminal aldehyde groups. This duality improves water permeability, resistance to organic fouling, and oil removal efficiency, showing notable rejection of larger anionic dyes. The innovative TTA-DFP-COF membrane meets pressing water purification needs, standing out for its synthesis speed, ease, and superior separation capabilities.

Keywords

Covalent Organic Frameworks (COFs), Membrane technology, Microwave-mediated interfacial polymerization, Surface properties control, Water treatment applications.

Introduction

Membrane technology has gained considerable attention in the field of filtration due to its ability to efficiently replace conventional energy-intensive separation techniques.[1,2] Developing membranes with a bottom-up approach and the flexibility to control their porous structure and surface properties could represent a breakthrough in many separation processes, particularly in water treatment.[3,4] Reticular materials, such as Metal-Organic Frameworks (MOFs) and Covalent Organic Frameworks (COFs), offer unprecedented opportunities in the bottom-up approach for membrane synthesis.[5-7] Their precisely tunable structures and self-assembling behavior enable the controlled arrangement of building blocks to create well-defined membrane structures with tailored properties.[8] COFs have emerged as an intriguing family of porous nanomaterials composed of cost-effective lightweight elements (C, N, O, B, etc.) that exhibit excellent structural diversity, tunable and permanent porosity, ordered structures, and high thermal and chemical stability.[9-11] These properties make COFs attractive for various applications such as gas adsorption, [12,13] water treatment,[14] energy storage,[15,16] sensing, [17,18] drug delivery,[19-23], and catalysis.[24,25] Most COFs synthesized by the conventional solvothermal procedure are obtained as insoluble powders. Many attempts have been made to develop COF-based membranes, including mixed matrix membranes and self-standing membranes by interfacial polymerization.[26-30] COFs-based mixed matrix membranes are easy to make, versatile, and could change the properties of polymeric membranes, but the porous structure of the polymeric matrix determines the filtration efficiency.[29] On the other hand, interfacial polymerization has been used to prepare self-standing COF membranes, but their synthesis is time-consuming and could take many days, and they are mostly grown as a thin film on a substrate (Table S1).[30] In addition, the poor solubility of most aromatic amine COFs' building blocks makes it challenging to apply interfacial polymerization for COF membranes' synthesis at a liquid-liquid interface.[31] Interfacial polymerization at the liquid-air interface has also been reported for the fabrication of self-standing COF membranes.[32,33] However, a Langmuir-Blodgett method was required to transfer the COF thin film from water to a substrate, and the process had to be repeated to obtain a robust COF filtration membrane. In addition, the COF monomers must have an amphiphilic nature to interpose between the organic phase and water interface. While synthesizing COFs as membranes is important, it is essential to ensure that the process is both rapid and straightforward, requiring as few steps as possible to enable large-scale production. Moreover, many studies on COF membranes focus on controlling their pore size,[34-36]

but reports on controlling the wettability of the membrane surface remain rare, even though it is one of the most important physicochemical properties of membranes.[37] The organic nature of COFs and their hydrophobicity make it challenging to modify the surface wettability of a COF membrane without changing its structure's building blocks, functionalizing it, or treating it post-synthetically, which could be time and energy-consuming. For this reason, most studies focusing on the surface wettability of COF membranes have attempted to produce superhydrophobic membranes or membrane coatings.[38,39] However, the studies in polymeric membranes are shifting to the fabrication of hydrophilic and superhydrophilic membranes and membrane coatings to increase water flux and reduce organic fouling of membranes, which is one of the major challenges for their commercialization.[40-42] Therefore, developing a fast and simple method to synthesize self-standing COF membranes with tunable hydrophilicity is challenging but essential for industrial membrane applications. Recently, a self-standing COF membrane was synthesized by covalently linking the building blocks at the liquid-solid interface and used for membrane distillation.[37] The surfaces of the membranes were then modified by a reverse imine-bond formation reaction to produce a hydrophilic surface, reduce membrane fouling, and increase water flux. However, the membrane preparation process takes up to 4 days, and treating it with an alkaline solution to obtain a hydrophilic surface takes an additional 18 to 24 hours, necessitating nearly 5 days to make the modified membrane. In another study, solvent-induced fragmentation was used to tune the surface wettability of a self-standing 3D COF membrane, resulting in a higher hydrophobicity of the membrane surface.[43] However, the membrane preparation takes two days, and the study focuses on hydrophobic and superhydrophobic COF membrane surfaces.

Here, we have achieved significant success by elaborating a series of dual superhydrophilic/near-hydrophobic self-standing imine-linked TTA-DFP-COF membranes. The breakthrough we have achieved in this study lies in the synthesis of a superhydrophilic/near-hydrophobic self-standing COF membrane in a one-step and rapid procedure with the ability to control the surface properties of the membrane without any post-synthetic modification and successfully use it for various wastewater treatment applications. This was made possible using a novel microwave-mediated interfacial polymerization method at the liquid-water vapor interface in a few minutes. The unique aspect is that while the side of the membrane in contact with water vapor is superhydrophilic, extending the reaction duration turns the side in contact with dioxane nearly hydrophobic. This synthesis duration is considerably shorter than previously reported COF membranes (Table S1).

Both surface chemistry and roughness contribute to this wettability variation, with the superhydrophilic side, when exposed to humid air, exhibiting a roughness reduced by a factor of ten. To delve into the membrane's molecular composition and structure, we used Raman, ATR-FTIR, XPS, AFM, and TEM. This revealed that the vapor-face's hydrophilic nature stemmed from the reaction between terminal -NH_2 groups of the triamine precursor and aqueous acetic acid. In contrast, the dioxane face was characterized by dominant terminal aldehyde groups, lending it a near-hydrophobic trait. Comprehensive characterization of the COF membrane demonstrated its crystallinity, stability, and adaptability in surface wetting. Our time-sensitive TEM/STEM analyses and morphological inspections highlighted the role of microwave activation in the synthesis. It fostered the mesoscale self-assembly of COF nanosheets at the liquid-vapor interface. Influenced by water condensation and focused microwave energy led to the emergence of a membrane with distinct face textures: a smooth superhydrophilic vapor-face and a textured near-hydrophobic dioxane-face. The formation of this thick membrane begins in a few minutes and continues to grow in bulk until the building components are consumed, allowing thickness control.

To put the COF membrane to the test, water filtration experiments were performed with salts, dyes, and mineral oil using vacuum filtration, and efficient filtration at a high water flux was observed. The results show that the rejection increases with the increase in the molecular size of the pollutants, suggesting that molecular sieving could have contributed to the rejection, in addition to electrostatic repulsion due to the negatively charged membrane surface. The superhydrophilicity of the membrane’s vapor face was also explored in oil-in-water emulsion filtration and showed an excellent oil rejection at high water flux. Furthermore, the membrane demonstrated potent antimicrobial and anti-biofouling properties against both gram-negative (*E. coli*) and gram-positive (*S. aureus*) bacteria while being biocompatible. This characteristic is crucial for water filtration membranes, as it enhances their effectiveness in preventing bacterial adhesion, inhibiting biofilm development, and ensuring consistent, uncontaminated water output. In light of global water challenges, our TTA-DFP-COF membrane offers a groundbreaking solution with immense potential for real-world water treatment applications, heralding a step forward in sustainable purification technologies. Our research stands out in the field due to our pioneering approach that combines microwave-assisted synthesis with a novel interfacial polymerization technique at the dioxane-water vapor interface. This innovative method endows the membranes with a dual character - balancing near-hydrophobic and hydrophilic properties - tailored specifically for water

treatment applications. Given that research on COF membranes is in its nascent phase, groundbreaking studies like ours are crucial for accelerating the advancement of this promising domain.

Results and Discussion

Membrane Synthesis and Characterization

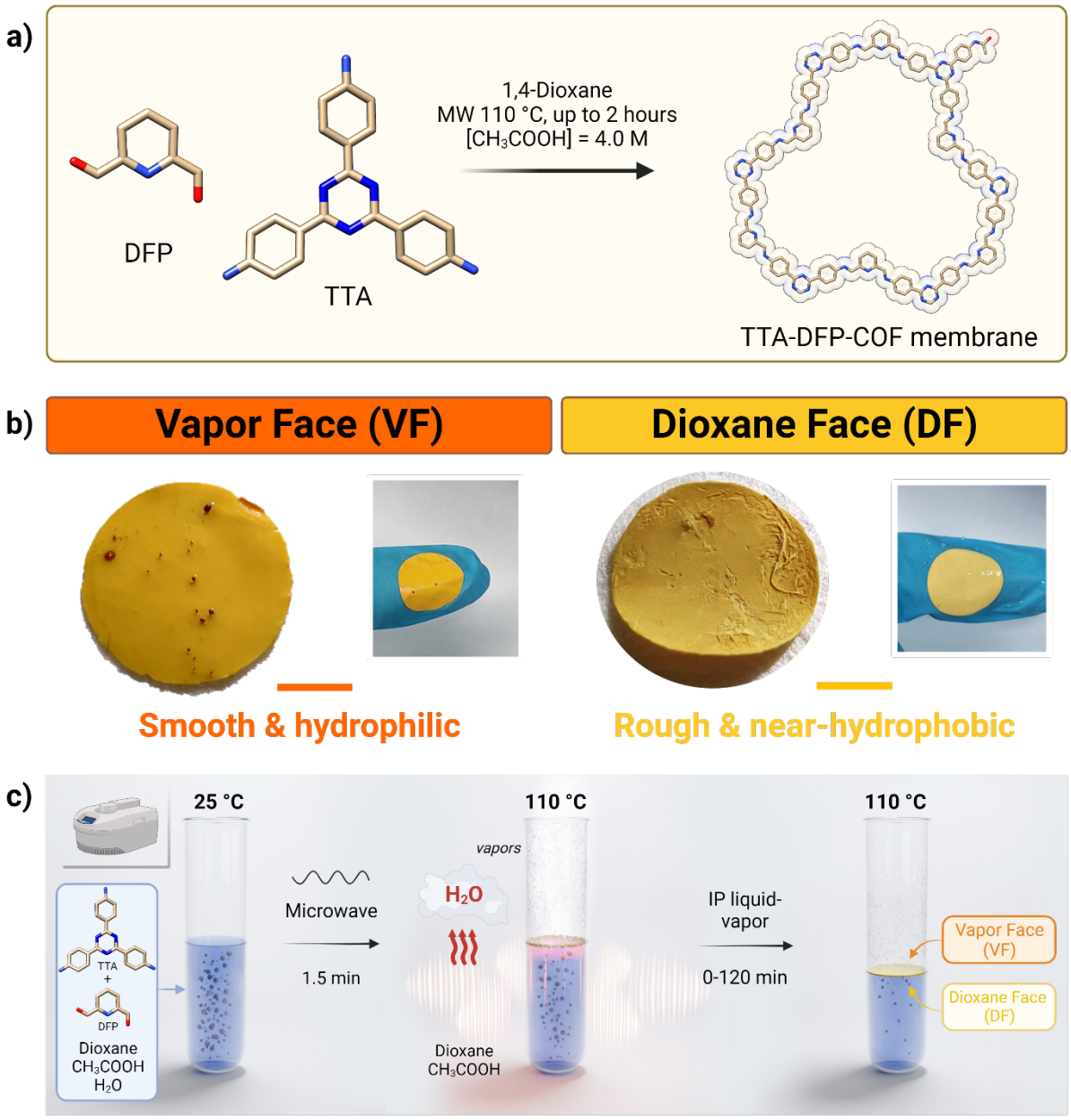

Figure 1. Interfacial polymerization (IP) at the dioxane–water vapor interface of a continuous, defect-free, highly crystalline, and porous self-standing COF membrane.

a) Chemical structure and synthesis pathway of the TTA-DFP-COF membranes obtained under microwave irradiation.

b) Digital images of the TTA-DFP-COF membrane: the vapor face is smooth and glossy in comparison with the rough and matte texture of the dioxane face. Scale bar = 1 cm.

c) Schematic representation of the membrane formation inside the microwave vessel. The self-standing TTA-DFP-COF membrane is formed due to the confinement of the polymerization of the aldehyde and amine monomers at the interface between dioxane and water vapors.

Self-standing COF membranes (denoted as TTA-DFP-COF membrane) with different thicknesses– 25, 55, and 85 μm– were prepared by covalently linking 2,6-diformylpyridine (DFP, 21 mg, 0.15 mmol, 5 equivalents) and 4,4',4''-(1,3,5-triazine-2,4,6-triyl)trianiline (TTA, 12 mg, 0.03 mmol, 1 equivalent), in 3 mL of anhydrous 1,4-dioxane and in presence of 0.5 mL of aqueous acetic acid (13 M, $[\text{acetic acid}]_{\text{final}}$ = 4.0 M) at 110 °C under microwave irradiations (Figures 1a and S1). The membrane formed at the liquid–vapor interface as observed in Movie 1. By adjusting the reaction time during microwave irradiation to 5, 45, and 120-minute intervals, we could control the thickness of the membrane. The membranes are denoted TTA-DFP-COF-**5**, TTA-DFP-COF-**45**, and TTA-DFP-COF-**120**, where **5**, **45**, and **120** represent the reaction time in minutes. After the specified reaction time, a free-standing membrane was obtained, showing no apparent cracks. The membrane displayed a smooth and glossy face on its upper side (contact with water vapors), referred to as the vapor face (VF), whereas the dioxane face (DF, contact with the solution) showed a rough and matte appearance (Figure 1b, Movie 2). Retrieving the membrane was easily accomplished using tweezers, and it could be cleaned multiple times with dioxane and ethanol (Movie 3). The membranes were stored in ethanol or water. Movies are attached in the Supplementary Information file.

In contrast to alternative methods for preparing COF membranes, our strategy stands out for its simplicity and speed. The preparation process of TTA-DFP-COF membranes can be completed in a few minutes, making it one of the fastest approaches for COF membrane preparation to date (Table S1). The linkers (DFP and TTA) are mixed in dioxane and sonicated for a few seconds to dissolve. Then, 0.5 mL of aqueous acetic acid (13 M, $[\text{acetic acid}]_{\text{final}}$ = 4.0 M) was added rapidly, and the mixture was placed immediately in the microwave oven to initiate heating (Figure 1c). The temperature quickly increases to 110 °C in 1.5 minutes. During the ramp, the 125 μL of water (from the aqueous acetic acid) starts boiling, and the first bubbles are observed around 80 °C after 40 seconds of ramping, and keep boiling for 30 seconds until 110 °C is reached (Movie 1). Water condensation can be observed on the vessel walls. The emergence of a film can be observed at the interface between the vapor and liquid phases. We previously demonstrated that at room temperature, a small amount of water favors the stacking of small nanosheets, leading to nanoparticle formation.[44]

Microwave (MW) energy revolutionizes chemical synthesis by directly energizing the sample for quicker, more even heating, making it highly effective for producing Covalent Organic Frameworks (COFs) with superior quality and efficiency.[45] Despite its advantages, reports on COF membranes synthesized via MW are lacking. Microwave irradiation is essential for TTA-DFP membrane synthesis; it causes water to evaporate and creates a vapor layer, enabling localized heating at the liquid-vapor interface, which is critical for the membrane's formation. Due to their distinct polar and ionic properties, solvents exhibit varying interactions when exposed to microwaves. Polar solvents like water exhibit efficient diffusion under microwave irradiation due to their high dielectric constants, interactions with electromagnetic fields, and dipolar characteristics. As a consequence, the temperature of the solvent rises significantly during this process. Non-polar solvents like dioxane can only be heated in the presence of other components in the reaction mixture that respond to microwave energy, such as water or acetic acid.[46] In such cases, it is possible to achieve high temperatures. In our particular situation, as water evaporates and re-condenses at the liquid-vapor interface, the conduction of microwave heating becomes locally significantly elevated. As a result, the focused application of heat at the dioxane-water vapor interface precisely moderates the diffusion of acetic acid, which in turn initiates the selective polymerization of unreacted DFP aldehyde groups, terminal aldehyde groups, and free amine groups on the nanosheets. This targeted polymerization at the interface culminates in the assembly of the COF membrane, a process depicted in Figure 1c and further elucidated in Movies 4 A, B, and C. Control experiments using an oven and an oil bath as heating source, as opposed to microwave irradiation, failed to produce membranes, yielding only powder, underscoring the essential nature of MW energy in this process (Figure S3). This process benefits from the absence of stirring, which ensures the undisturbed distribution of the various solvents. As a result, the heating energy is not uniformly distributed throughout the mixture but concentrates in areas with more polar solvents. The control experiment with stirring did not lead to membrane formation, showing the primordial role of not disturbing the solvent post-organization (Movie 5). The control experiment with dry acetic acid did not lead to membrane formation, showing water’s primordial role in the mechanism. Upon the initiation of membrane polymerization, prolonging the duration results in accumulating additional thin layers of COF beneath the existing ones, ultimately augmenting the overall thickness of the membrane.

FTIR and solid-state NMR spectroscopies were used to analyze the chemical composition of the TTA-DFP-COF-**5/45/120** membranes. The findings revealed that all the membranes exhibited identical patterns regarding their characteristics independently of their thickness.

FTIR analysis offered detailed insights into the molecular architecture of the newly synthesized imine COF membrane. The monomers exhibit unique spectral features, with amine monomers (TTA) showing NH_2 stretching vibrations in the 3460–3320 cm^{-1} range and aldehyde monomers (DFP) characterized by a C=O stretch at 1711 cm^{-1} (Figures S4-5). The transition to imine COFs was marked by the NH_2 peak's disappearance, reduction in the C=O signal, and emergence of an imine C=N stretch at 1621 cm^{-1}—proof of polycondensation. Additional spectral features included a C=N stretch at 1507 cm^{-1}, a broad C-N peak at 1364 cm^{-1} related to the triazine core, and a C=C stretch at 1580 cm^{-1}.[47] The spectrum further revealed a faint C=O band at 1706 cm^{-1} from residual aldehydes and a distinct amide C=O stretch at 1680 cm^{-1}, with accompanying amide C-N stretching at 1242 cm^{-1} and C-N-C stretching at 1325 cm^{-1}. These bands suggest the formation of terminal N-phenyl acetamide groups, likely from the TTA precursor reacting with acetic acid, illustrating the nuanced chemical interactions within the COF structure.

^{13}C CP-MAS solid-state NMR spectroscopy was employed to study the chemical environment at the atomic level of the obtained TTA-DFP-COF membranes (Figure S7). The ^{13}C CP/MAS solid-state NMR spectrum obtained from TTA-DFP-COF membranes (Figure S7a) is well resolved and reveals mainly peaks appearing from the aromatic (100 to 150 ppm) and aromatic imine carbon atoms (150 to 175 ppm). The formation of the new imine bond is confirmed by the new peak appearing at ~160 ppm. The spectrum is also characterized by the presence of terminal aldehyde groups appearing at ~ 194 ppm. Chemical shift assignments were further confirmed by recording the solid-state NMR spectra of starting materials (TTA and DFP) and final TTA-DFP COF membranes (Figure S7b).

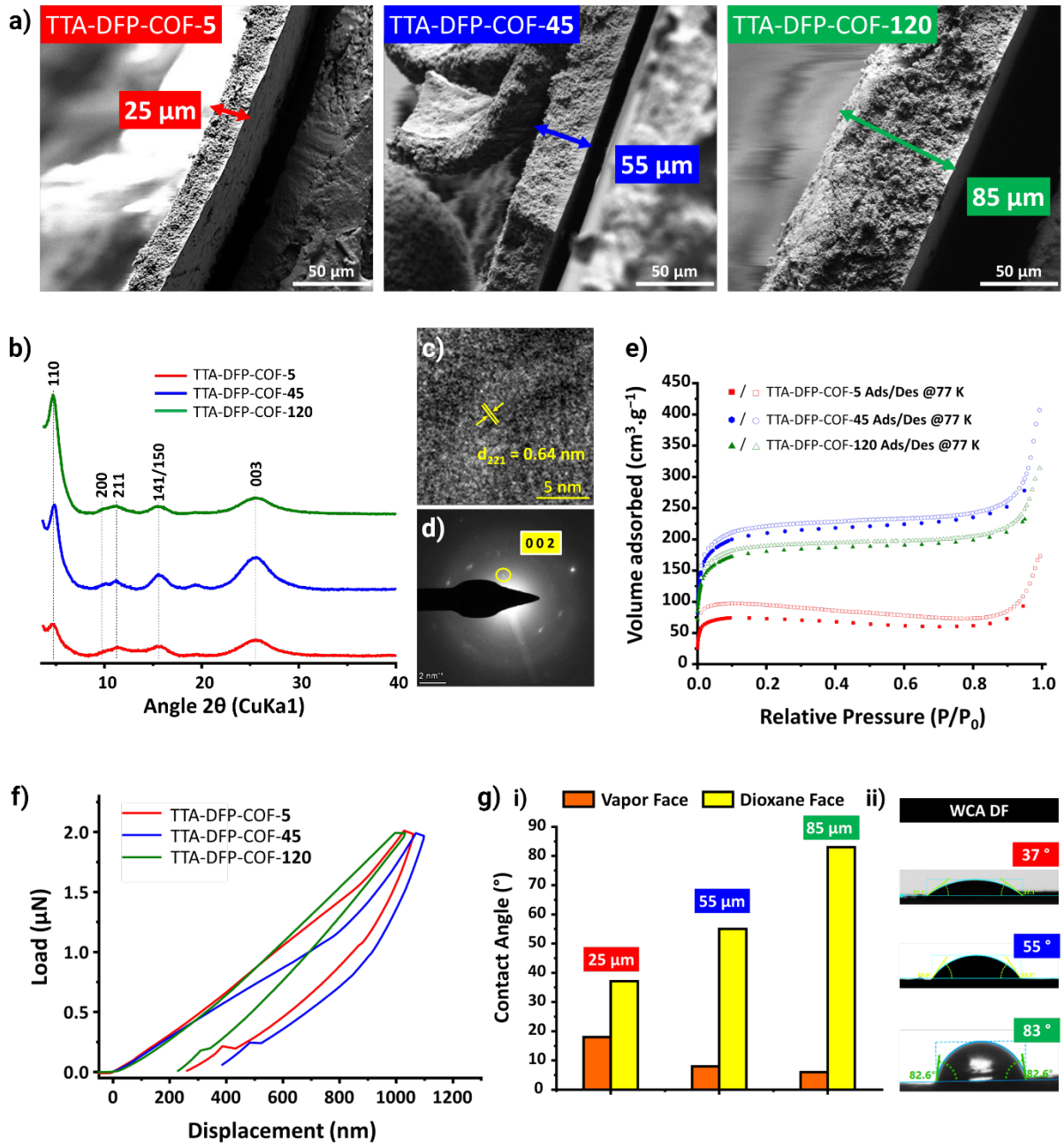

Figure 2. Structural characterization of the TTA-DFP-COF membranes.

a) SEM Cross-sectional images of TTA-DFP-COF-**5**, TTA-DFP-COF-**45**, and TTA-DFP-COF-**120**.

b) PXRD of TTA-DFP-COF-**5** (red), TTA-DFP-COF-**45** (blue), and TTA-DFP-COF-**120** (green). HRTEM analysis of TTA-DFP-COF-**120** confirming the material's crystallinity:

c) HR-TEM image displaying lattice fringes (lattice fringe distances d = 0.64 nm) corresponding to the (221) plane of the COF.

d) Selective area electron diffraction (SAED) images indicate the TTA-DFP-COF membrane's high crystallinity well matching to d_{002} plane with d-spacing of 5.1 Å.

e) N_2 adsorption isotherms, and f) representative indentation load versus surface penetration depth (P-h) curves of TTA-DFP-COF-**5** (red), TTA-DFP-COF-**45** (blue), and TTA-DFP-COF-**120** (green).

g) Surface wettability analysis:

i) Water contact angle (WCA) of the vapor (VF, orange) and dioxane (DF, yellow) faces of TTA-DFP-COF-**5** (red), TTA-DFP-COF-**45** (blue), and TTA-DFP-COF-**120** (green), and

ii) corresponding WCA digital images of the DF of TTA-DFP-COF-**5/45/120**.

Table 1. Physicochemical properties of TTA-DFP-COF-**5/45/120** membranes; TPV: total pore volume, WCA: water contact angle, VF: vapor face, DF: dioxane face.

	TTA-DFP-COF-**5**	TTA-DFP-COF-**45**	TTA-DFP-COF-**120**
Thickness (µm)	24.8 ± 1.6	55.1 ± 1.8	85.7 ± 2.6
BET (m^2g^{-1}), (TPV*, cm^3g^{-1})	300, (0.11)	809, (0.39)	690, (0.33)
Pore Width (Å)	12.3/14.8	10.2	10.2
Young Modulus (MPa)	300 ± 100	500 ± 100	2100 ± 50
Hardness (MPa)	250 ± 50	350 ± 50	520 ± 100
WCA, VF/DF (°)	18/37	8/55	6/83

Subsequently, we analyzed the variances among the TTA-DFP-COF-**5/45/120** membranes through SEM, PXRD, HRTEM, and N_2 adsorption techniques. Additionally, we examined the membranes' mechanical properties and surface wettability, which were influenced by variations in their thicknesses.

The inner morphology and thickness of TTA-DFP-COF membranes were investigated by SEM (Figures 2a and S12-16). The TTA-DFP-COF-**5/45/120** membranes display two distinct types of faces (Figures S14-16). The vapor face (VF), which was exposed to water vapor during synthesis, appears smooth, compact, and continuous. In contrast, the dioxane face (DF) appears rough. Notably, both faces are free from any cracks. As the reaction time increases, the contrast in characteristics between the VF and DF faces becomes more distinct (Figures S14-16). The inner structure of the TTA-DFP-COF-**5/45/120** membranes is made of a laminated arrangement consisting of multiple sheets, each measuring 5-10 μm (Figure S16-17). These sheets were stacked on top of one another, creating the characteristic structure shown in Figure S16. As the reaction time increased, the thickness of the membranes also increased, reaching 25 μm, 55 μm, and 85 μm for TTA-DFP-COF-**5**, TTA-DFP-COF-**45**, and TTA-DFP-COF-**120**, respectively, as observed using cross-section SEM (Figures 2a and S12-13).

The crystalline structure of TTA-DFP-COF membranes was characterized using powder X-ray diffraction (PXRD), revealing clear evidence of crystallinity through distinct (110) Bragg diffraction peaks at $2\theta = 4.8°$. Additional peaks at $2\theta = 9.8°$, 11.2°, and 15.5° correspond to the (200), (211), and combined (141) and (150) planes, respectively, alongside a higher-order peak at $2\theta = 25.5°$ for the (003) plane (Figures 2b and S19). These PXRD patterns match the simulated data (Figure S19), confirming the material's structural integrity with an interplanar π–π stacking distance of 3.5 Å, consistent with theoretical models. The analysis also indicates that membrane thickness influences microstructural features like crystal packing, with thicker membranes showing stronger diffraction peak intensities, implying better crystallinity and internal order. This is demonstrated by the intensities of the (110) peak increasing with thickness, noted at 4800, 16100, and 19000 arbitrary units for membranes of varying thicknesses, with a significant rise in peak intensity observed as thickness increases from 25 μm to 55 μm before stabilizing between 55 μm and 85 μm (Figure S27).

HRTEM was then used to acquire insights into the interior structure and the crystallinity of the COF membranes. Images show a highly ordered arrangement composed of a multilayered structure of individual COF nanosheets (Figures 2 c-d and S20-21), self-assembled due to interlayer π-π stacking with independent lattice fringes. Lattice-resolution TEM images of exfoliated TTA-DFP-COF membrane suggested that they are crystalline with consistent and continuous lattice fringes that extend throughout the COF (Figures 2 c and S22). The lattice spacings were 3.4 and 6.4 Å, as measured by fast Fourier transform, which match the expected d_{003} and d_{221} spacings, respectively. Furthermore, the selected area electron diffraction (SAED, Figures 2 d and S23) demonstrates the well-crystallized feature of the TTA-DFP-COF membrane, which exhibited distinct electron diffraction spots, well matching to d_{002} plane with *d*-spacing of 5.1 Å.

The TTA-DFP-COF-**5/45/120** membranes demonstrated permanent porosity, as shown by low-pressure N_2 adsorption experiments that yielded fully reversible type-I isotherms, indicative of nitrogen condensation within the membranes' interstitial voids (Figure 2e, Table 1). The Brunauer-Emmett-Teller (BET) surface areas were calculated to be 300, 809, and 690 m^2/g, with corresponding total pore volumes of 0.11, 0.39, and 0.33 cm^3/g for the TTA-DFP-COF-**5/45/120** membranes, respectively (Figure S26). This data aligns with PXRD findings that indicated an increase in (110) peak intensity with membrane thickness up to 55 µm, after which it plateaus (Figure S27). This trend hints at the effect of microstructural differences on the surface area despite a consistent crystalline structure (Figure S27). Pore size analysis showed TTA-DFP-COF-**5** with the largest average pore size (12.3 Å), contrasting with the smaller, uniform pore sizes (10.2 Å) of TTA-DFP-COF-**45** and TTA-DFP-COF-**120** (Figure 26). These physical attributes, including BET surface areas and pore distributions, reflect the membranes' crystallinity levels, which are influenced by the synthesis conditions such as reaction time, impacting membrane thickness and packing. Echoing research by Ma *et al.* that connects COF crystallinity to sorption properties,[48] our findings underscore the importance of synthesis precision in optimizing COF membranes for specific uses, enhancing our grasp of COF membrane fabrication.

Through our interfacial polymerization technique, we successfully obtained flexible and continuous TTA-DFP-COF membranes with a diameter of 2.5 cm. These membranes exhibit good mechanical strength, facilitating their extraction from the mother solution and transfer onto diverse substrates (Movie 3). Therefore, the quantitative nanomechanical properties, Young's modulus

(*Er*), and hardness (*H*) were calculated based on the as-obtained load/depth curves (Figures 2f and S28, Table 1). The TTA-DFP-COF-**120** showed the highest values for both parameters (*Er* = 2100 MPa and *H* = 520 MPa) among the three membranes (*Er* = 300 MPa and *H* = 250 MPa for the TTA-DFP-COF-**5**; *Er* = 500 MPa and *H* = 350 MPa for the TTA-DFP-COF-**45**). TTA-DFP-COF-**120** membrane demonstrates excellent mechanical properties (Table S2 for comparison with other COF membranes). Even after drying, the self-standing COF membranes could maintain their flexibility and integrity, which strongly verifies their mechanical robustness (Movie 6). Consequently, it is well-suited for water filtration applications.

In order to explore the properties of the surface hydrophobization and wettability of the TTA-DFP-COF-**5/45/120** membranes, we conducted measurements of the water contact angle (WCA) on both the VF (exposed to water vapors) and DF (exposed to dioxane) faces while considering the variations in membrane thickness (Figures 2g and S29). Significant differences in behavior were observed between the VF and DF faces of the membranes, as well as function of the thickness.

Upon immediate observation, the vapor face of the TTA-DFP-COF-**5/45/120** membrane experienced almost complete wetting by water droplets, particularly in the case of TTA-DFP-COF-**120** with a WCA of 5.9°, as indicated in Table 1 and shown in Figures 2g and S29. In contrast, the hydrophilicity of the dioxane face decreased relative to the membrane's thickness and roughness. The contact angle exhibited an increase, reaching values of 37.1°, 55.0°, and 82.6° (almost hydrophobic) for TTA-DFP-COF-**5**, TTA-DFP-COF-**45**, and TTA-DFP-COF-**120**, respectively. Notably, the TTA-DFP-COF-**5/45/120** membranes displayed divergent face characteristics based on thickness. While one face demonstrated a markedly superhydrophilic nature, the other exhibited near-hydrophobic properties. Significantly, the differences in morphology were less evident in the case of TTA-DFP-COF-**5** aligning with the trend of fewer disparities between the two faces, as indicated by water contact angles (WCA) measurements.

This duality in faces behavior offers distinct advantages: the superhydrophilic face promotes the high water permeance, increased resistance to organic fouling compared to traditional polymeric membranes, while facilitating rapid and efficient removal of oil or organic residues from oil-in-water suspensions. The near-hydrophobic face, on the other hand, could potentially promote anti-fouling properties for inorganic species while still allowing good water permeation. This approach

also opens the door to the development of fabrication protocols for COF membranes with different wettability behaviors on each side where the hydrophobic side has a higher water contact angle. In this case, the other surface could facilitate the usage of the membranes in other applications, such as oil purification from water and seawater desalination using membrane distillation, mimicking the properties of traditional polymeric Janus membranes.[49]”

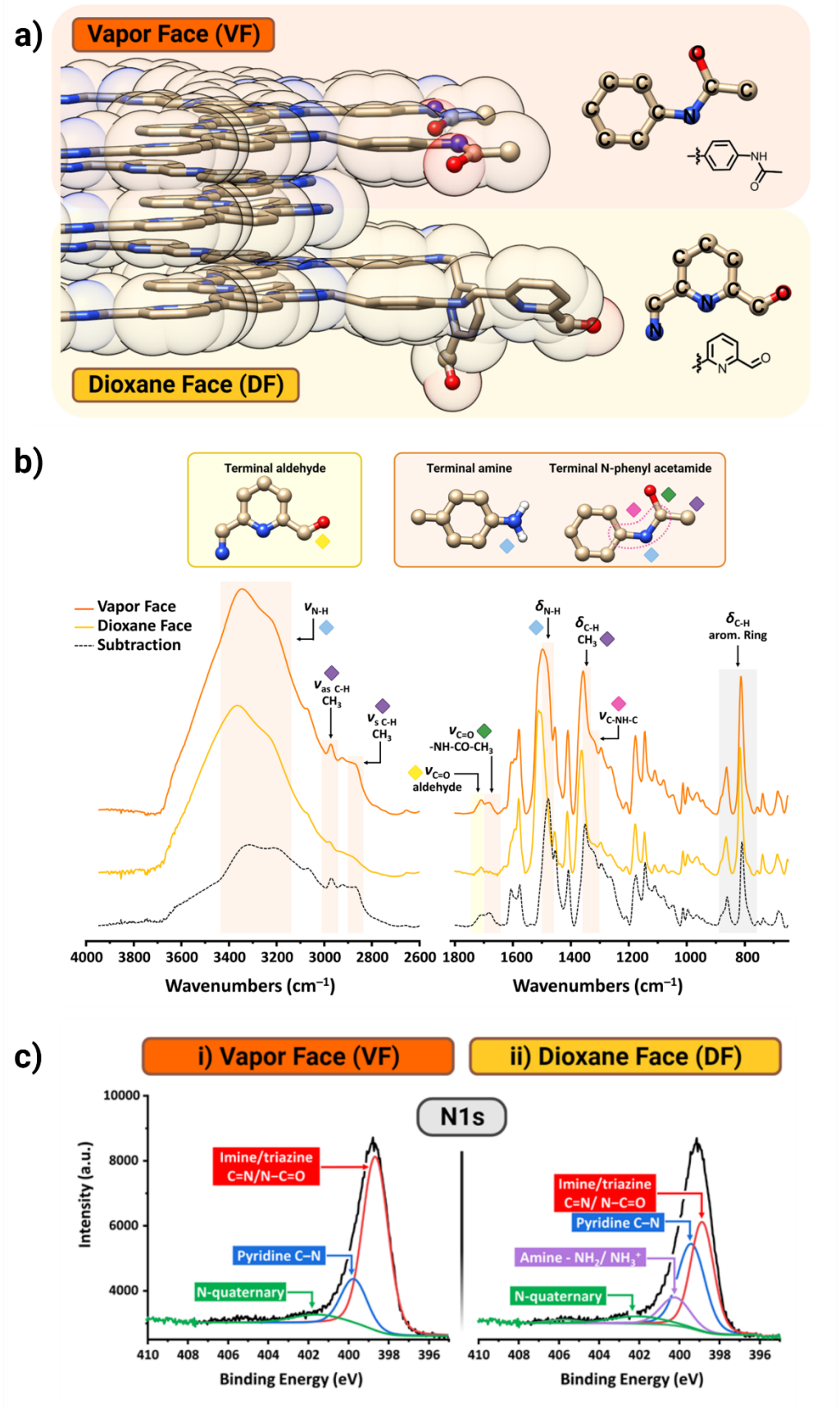
a)
Vapor Face (VF)
Dioxane Face (DF)
b)
Terminal aldehyde
Terminal amine
Terminal N-phenyl acetamide
Vapor Face
Dioxane Face
Subtraction
Wavenumbers (cm⁻¹)
Wavenumbers (cm⁻¹)
c)
i) Vapor Face (VF)
ii) Dioxane Face (DF)
N1s
Intensity (a.u.)
Imine/triazine C=N/N–C=O
Pyridine C–N
N-quaternary
Amine - NH2/ NH3+
Binding Energy (eV)
Binding Energy (eV)

Figure 3. The dual hydrophobic and hydrophilic behavior of the TTA-DFP-COF membrane is mainly due to the favorable orientation of the hydrophilic NH_2/ NH-CO-CH_3 groups towards the vapor face and the aldehyde toward the dioxane face.

a) Schematic representation of the species distribution within the vapor (VF) and dioxane (DF) face of the membrane.

b) ATR-FTIR spectra of VF (hydrophilic, orange) and DF (nearly hydrophobic, yellow) of the TTA-DFP-COF membrane and their corresponding subtraction (black).

c) XPS N 1s spectra of VF (i) and DF (ii) of the TTA-DFP-COF membrane.

We investigate the reason behind the membranes' dual near-hydrophobic and hydrophilic properties. The micro/nanotextures and chemistry of the membrane's surface affect hydrophobization and wettability.[50,51] Hydrophobization and wettability of a solid surface are primarily determined by its chemical composition. Polar groups such as COOH, OH, and NH_2 lead to surface hydrophilicity, while non-polar groups such as CH_3 or CF_3 will make the surface hydrophobic.[52]

Using a combination of spectroscopic techniques (Raman, ATR-FTIR, and XPS), we examined the TTA-DFP-COF-**120** membrane faces. Atomic force microscopy (AFM) was additionally employed to analyze their textures. This approach was chosen because SEM investigations (as shown in Figures 2a and S12-16) revealed noticeable variations in morphology between the two surfaces, especially when exposed to prolonged reaction durations (Figure 3a).

Figure S30 displays the direct Raman spectra of the vapor and dioxane faces and their corresponding subtraction. The primary distinction between the VF compared to the DF one lies in the regions associated with the C-H vibrations of the aromatic ring, and the C-H vibrations of a methyl group, and possible C-N vibration of the imine group. However, the difference between these two faces was not easily observed as the excitation laser's penetration depth, even after adjusting the focal length, could also limit the discrimination of the two faces.

Consequently, Attenuated Total Reflection Fourier Transform IR (ATR-FTIR) spectroscopy was used as an alternative as the penetration depth of the evanescent IR beam is typically on the order of a few micrometers (around 3 μm), making ATR particularly suitable for the qualitative analysis of surface layers of TTA-DFP-COF membrane. Consequently, the analysis is not exclusively confined to the external surface of both faces but part of the bulk as well. This justifies the similar positions of some bands on both sides, however, with different relative intensities (Figure 3b).

The ATR-FTIR spectra of the VF and DF and their corresponding subtraction are given in Figure 3b and Table S3. The spectrum of the VF reveals distinct higher absorption bands at 3400-3200 cm^{-1} (N-H stretching), 2977 and 2868 cm^{-1} (C-H asymmetric and symmetric stretching of the CH_3 group, respectively), 1680 cm^{-1} (C=O stretching of -NH-CO-CH_3), 1480 cm^{-1} (N-H bending), 1350 cm^{-1} (C-H bending), and 1325 cm^{-1} (C-N-C stretching). These bands provide evidence of terminal N-phenyl acetamide (phenyl-NH-CO-CH_3) groups. These groups are most likely formed

by a reaction between certain terminal -NH_2 groups of TTA precursor and aqueous acetic acid (CH_3COOH). This allows us to propose that the terminal group of the VF is mainly -NH_2 and amide TTA precursor, preferentially interacting with the aqueous phase. In contrast, these groups are either absent or present with significantly low intensity in the FTIR spectrum of the DF. Instead, the predominant feature observed on the DF of the TTA-DFP-COF membrane is the presence of terminal aldehyde groups, in which a distinctive band can be identified at 1710 cm^{-1}. The terminal aldehyde groups from DFP molecules predominantly interact with the dioxane solvent. This distinction in terminal groups on the membrane's faces explains the TTA-DFP-COF membrane's dual hydrophobic and hydrophilic properties, with the NH_2/ NH-CO-CH_3 groups being notably more hydrophilic than the aldehyde groups.

To understand how TTA's -NH_2 groups react with acetic acid, a control experiment mirroring the membrane synthesis conditions was performed, aiming to produce N-phenyl acetamide. The formation of this compound was verified through ^{1}H NMR, ^{13}C CP/MAS solid-state NMR, and FTIR spectroscopy, revealing peaks indicative of amide bond creation (section 3.2 in SI). These results confirm the reaction pathway where TTA's primary amine groups bond with acetic acid to form amide linkages.

The high-resolution XPS survey spectra confirm that the TTA-DFP-COF membrane's faces are predominantly composed of carbon, nitrogen, and oxygen elements, with the vapor face (VF) showing a greater oxygen content at 6.7%, compared to 3.6% on the Dioxane face (DF) as detailed in Figure S31 and Table S4.

Analysis of the C 1s signal reveals four distinct carbon environments corresponding to C=C (approx. 285.0 eV), C–N (approx. 285.8 eV), C−N=C/N−C=O amide (approx. 286.9 eV), and C=O from terminal aldehyde (approx. 288.5 eV) (Figure S32). Notably, the aldehyde C=O is more prevalent in the DF at 5.0%, in contrast to 3.6% in the VF, indicative of terminal aldehyde presence as listed in Table S5. Moreover, the amide's N−C=O signal is significantly stronger in the VF at 21.4%, versus 16.4% in the DF, suggesting a more substantial interaction and subsequent amide formation on the VF due to the reaction of terminal -NH_2 groups from the TTA precursor with aqueous acetic acid.

The N 1s and O 1s peaks demonstrate notable differences between the two faces. The DF's N 1s spectrum can be deconvoluted into four peaks that signify various nitrogenous entities, including to imine/triazine C=N/ N−C=O (~399.1 eV), pyridine C–N (~399.9 eV), amine -NH_2/ NH_3^+ (~400.6 eV), and N-quaternary (pronated pyridine, ~402.5 eV),[53] as shown in Figure 3c, S32 and Table S6. In contrast, the VF lacks amine species while showing a heightened presence of imine/triazine and amide structures, accounting for 50.0 % of the N 1s signal, which is an increase from the 37.5 % observed on the DF. This disparity supports the formation of amide linkages on the VF, as depicted in Figure S32, Table S6.

The DF's O 1s signal separates into two peaks related to the -C=O of -NH-CO-CH_3 and the -C=O of terminal aldehyde groups in DFP molecules, with respective contributions of 57.4 % and 38.2 %. On the VF, the dominance of the -NH-CO-CH_3 at 85.2 % corroborates the hypothesis of a condensation reaction between the TTA's terminal -NH_2 groups and aqueous acetic acid, while the diminished presence of -C=O from DFP at 14.8 % suggests a selective orientation towards the dioxane phase, as further detailed in Figure S32 and Table S7.

We subsequently conducted surface ζ-potential measurements on both faces. As anticipated, the VF displayed a notably more negative ζ-potential (−28 mV) than the DF (−10 mV). This difference can be attributed to the higher presence of terminal N-phenyl acetamide (phenyl-NH-CO-CH_3) groups on the VF. These groups have a polar C=O bond, which can lead to a net negative charge distribution, making them more polar than the aldehydes present on the DF (Figure S33). The density of these N-phenyl acetamide groups, as well as other possible molecular interactions, such as hydrogen bonding on the VF, might also play a role in this observed disparity.

In summary, the XPS and ζ-potential results align with the data gathered from ATR-FTIR analysis. The terminal aldehyde groups tend to orient themselves towards the DF, whereas the residual NH_2 groups of TTA predominantly react with COOH from acetic acid on the membrane's vapor face. The resulting condensation elucidates the dual hydrophobic and hydrophilic characteristics of the TTA-DFP-COF membrane from the chemical distribution aspect.

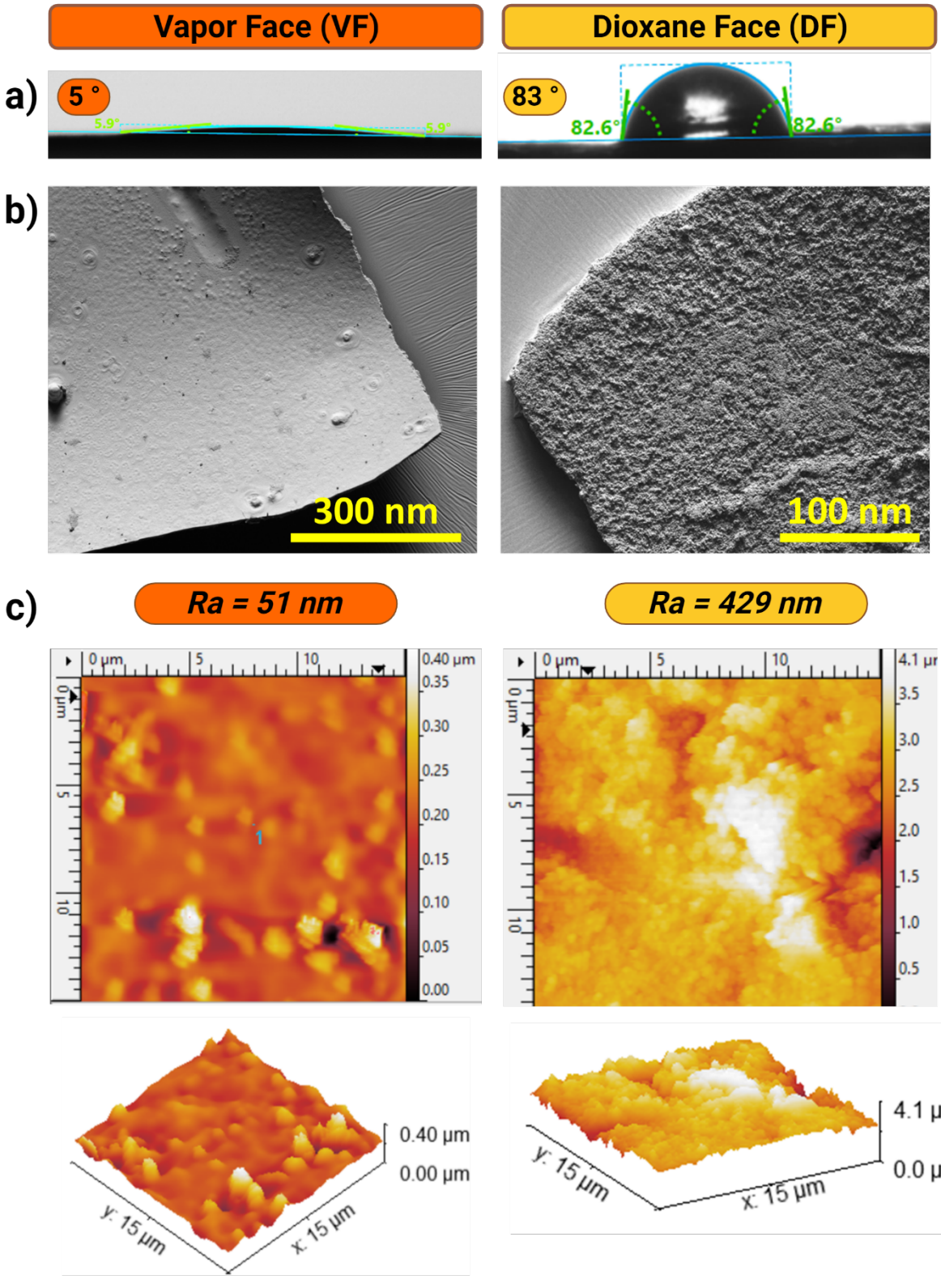
Vapor Face (VF)
Dioxane Face (DF)
a)
5 °
5.9°
5.9°
83 °
82.6°
82.6°
b)
300 nm
100 nm
c)
Ra = 51 nm
Ra = 429 nm
0 µm
5
10
0.40 µm
0.35
0.30
0.25
0.20
0.15
0.10
0.05
0.00
4.1 µm
3.5
3.0
2.5
2.0
1.5
1.0
0.5
0.40 µm
0.00 µm
y: 15 µm
x: 15 µm
4.1 µm
0.0 µm
y: 15 µm
x: 15 µm

Figure 4. The increased roughness observed on the DF of the TTA-DFP-COF membrane amplifies the effects of its inherent surface chemistry.

a) Digital images of the water contact angle,

b) SEM, and

c) AFM images of VF (left panel, orange) and DF (right panel, yellow) of the TTA-DFP-COF membrane. R*a* = roughness average.

Moreover, in 1936, Wenzel[54] established the correlation between roughness and hydrophobization/wettability, stating that introducing surface roughness would amplify the hydrophobization/wettability induced by the surface chemistry. [51,52]

The dioxane face (DF) of the membranes is near-hydrophobic and appeared rough upon visual inspection and closer SEM examination (Figures 4 a,b, and S12-16). In contrast, as mentioned previously, the superhydrophilic VF displayed a relatively smoother surface. Therefore, the surface morphologies of the membrane's vapor and dioxane faces were examined using AFM, enabling us to quantify their surface roughness factor, denoted as R*a* (roughness average). The hydrophilic VF displays a comparatively even surface with minimal folds and irregularities, indicated by an average surface roughness value of R*a* = 51 nm (Figure 4c). As a result, the VF showed a mirror-like shiny surface. On the other hand, the DF, which is hydrophobic, demonstrates significant fluctuations with an average surface roughness of R*a* = 429 nm. The roughness factor between the two sides is nearly ten times higher, highlighting a substantial difference in surface roughness.

The increased roughness on the DF side of the TTA-DFP-COF membrane enhances its unique surface chemistry, particularly the dominant terminal aldehyde groups, making it near-hydrophobic and affecting the wettability contrast between its two sides.[51,52] This difference in wettability is further shaped by how the membrane's functional groups are oriented and react; specifically, the terminal aldehyde groups are primarily found on the DF, whereas the NH_2 groups from TTA on the VF side undergo a condensation reaction with COOH from acetic acid. Such interactions elucidate the membrane's ability to exhibit both near-hydrophobic and hydrophilic properties.

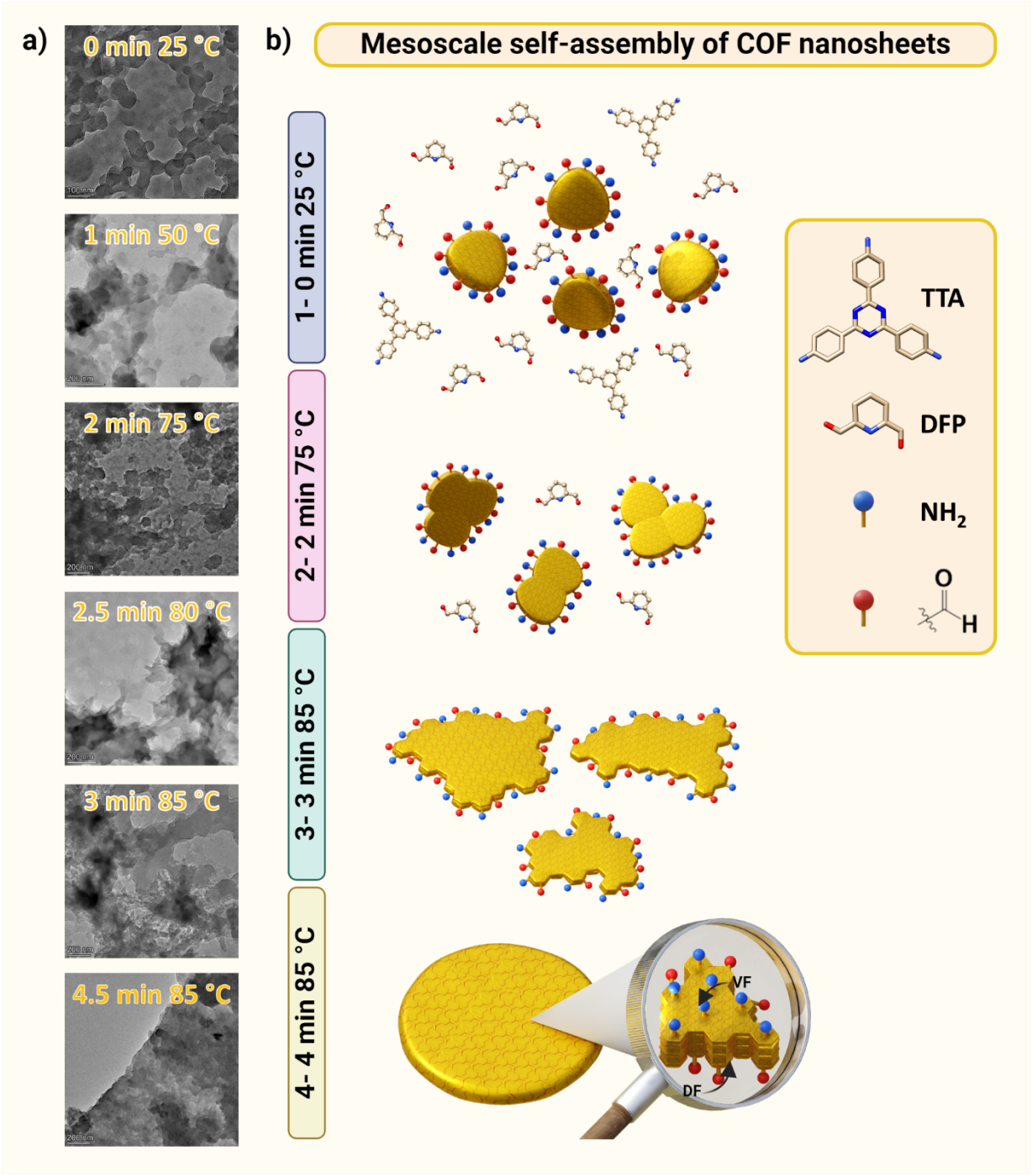

Figure 5. Covalent self-assembly of nanosheets at the interface between dioxane and water vapors transforms them into a self-standing COF membrane.

a) Time-dependent study of the membrane formation visualized by TEM of each step during the synthesis taken at different time intervals. Time is counted after the addition of acetic acid.

b) Illustrative depiction of the mesoscale covalent self-assembly process resulting in a crystalline, porous membrane. The unreacted DFP and terminal aldehyde groups on the nanosheet edges facilitate the assembly through reactions with free amines on the surface. As the COF nanosheets come together at the dioxane-water vapor interface, their peripheral aldehyde and amine groups link via Schiff base reactions. **Step 1:** 0 min, room temperature – rapid imine condensation produces crystalline COF nanosheets. **Step 2:** 2 min, 75°C – mesoscale assembly commences at the interface. **Step 3:** 3 min, 85°C – the nanosheets coalesce into expansive branched structures. **Step 4:** 4.5 min, 85°C – a robust membrane forms, composed of layered COF sheets, exhibiting a smooth vapor-facing side (VF) and a textured dioxane-facing side (DF), exemplifying the tailored polymerization and morphological development steered by the interface-specific microwave energy application.

In order to understand how the membrane forms when microwave activation is employed and the reason behind the difference in roughness between faces, we executed a time-dependent TEM/STEM study during the synthesis by dipping TEM grids at the liquid/vapor interface inside the microwave oven and performed a morphological analysis (Figures 5a and S34-37). The synthesis was slightly altered to slow the reaction kinetics and simplify the experimental process. We conducted the experiment in an open vessel mode, dipping the grid at various time intervals inside the oven. To prevent water evaporation as the system was no longer sealed, we reduced the reaction temperature to 85 °C. By decreasing the temperature, we achieved a slower reaction rate without affecting its overall outcome.

In the reaction, the amine (TTA) is used in default amounts, while the aldehyde (DFP) is in excess. The introduction of aqueous acetic acid ($[\text{acetic acid}]_{\text{final}}$ = 4.0 M) triggers a rapid imine condensation reaction at room temperature in solution (Figure 5b, **step 1**). This reaction quickly consumes a significant portion of the TTA, forming distinct crystalline nanosheets of COF (Figures 5a and S27-29, t = 0 min post-acid addition, 25 °C).

The rapid temperature increase induces the mesoscale self-assembly of COF nanosheets that occurs at the liquid-vapor interface due to two interconnected phenomena: water condensation at the liquid-vapor interface and concentrated microwave energy on the top (Figures 1c and 5b). The vapor water layer is critical because it allows slow diffusion of the acetic acid (demonstrated through ATR-FTIR and XPS) to the interface and induces the confinement of the polymerization of free −CHO aldehyde (unreacted DFP) and terminal aldehyde groups and free $-NH_2$ amines on the nanosheet surface at the interface between dioxane and water vapors (Figure 5b, **step 2**).

As a result, the nanosheets form larger structures (Figures 5a, **step 3** and S27-29, t = 1.5 min post-acid addition). Over time, branching occurs between these star-like structures, bringing them closer together. The structure becomes more ordered through a reorganization with improved stacking and increased transparency due to enhanced π-π stacking (Figures 5a, b and S27-29, t = 2-3 min post-acid addition). After approximately 4 minutes, a thick membrane is formed as COF layers continue to accumulate **(step 4)**. This layer-by-layer growth continues until the DFP linker is completely consumed and no more free aldehydes or amines are available. As a result, the VF is

smooth due to the COF nanosheet's continuous reorganization, while the DF is rough and full of aggregates, as observed using SEM attributed to the end of the process.[55]

Through time-dependent TEM/STEM studies and morphological observations, it was determined that the use of microwave activation in synthesis encourages the mesoscale self-assembly of COF nanosheets at the liquid-vapor interface. This process, influenced by water condensation and microwave energy concentration, results in the formation of a thick membrane with a smooth vapor face and a rough dioxane face due to differing organizational structures at each interface. The smoothness of the VF membrane results from microwave-assisted interfacial polymerization in the presence of water vapor, which ensures a controlled and even polymerization, yielding a homogenous and smooth COF layer. On the other hand, the DF membrane, formed in contact with dioxane, undergoes a less consistent polymerization due to variable reactant distribution and microwave energy, leading to a rougher texture.[56] These textural differences significantly affect the membrane's functionality, particularly influencing wettability and separation efficiency. The change in surface roughness, by a factor of ten, alongside chemical composition modifications, is the key to the varied wettability observed. The distinctive textures of VF and DF are central to the membrane's specialized separation properties and efficiency in water treatment applications.

For the rest of the study, we focused our attention on the TTA-DFP-COF-**120** membrane (85 µm), which shows excellent crystallinity, high surface area (690 m^2 g^{-1}), the highest mechanical properties as well as the highest discrepancy between superhydrophilicity and near-hydrophobicity of the two faces.

Ensuring the physical and chemical stabilities of the TTA-DFP-COF membrane is crucial to guarantee its effective utilization in real-world environments. The thermal stability of the COF membrane was measured by thermogravimetric analysis under nitrogen (Figure S38). TTA-DFP-COF membranes are thermally stable up to 450 °C without apparent weight loss, which meets the requirement of water treatment application.

Furthermore, the chemical stability of the TTA-DFP-COF membrane was evaluated upon their immersion for 24 hours in acidic, neutral, and basic (pH = 5, 7, and 9) aqueous solutions and common organic solvents (ethanol, dioxane, acetone, and dichloromethane, Figures S39-43). The TTA-DFP-COF membrane exhibited excellent chemical stability as it retained its integrity without

any visible delamination or alterations in its chemical structure after being immersed in various conditions for 24 hours. The lack of significant changes was confirmed through visual inspection (Figure S39), FTIR (Figures S40-41), and PXRD (Figures S42-43) analysis, highlighting the membrane's robust chemical stability. The high structural stability of the TTA-DFP-COF skeleton is attributed to the stable backbone, which prevents hydrolysis of the imine nitrogen.[57,58] Due to their exceptional stability, TTA-DFP-COF membranes are well-suited for fulfilling the application needs of molecular sieving and oil removal from water.

Membrane Filtration Performance

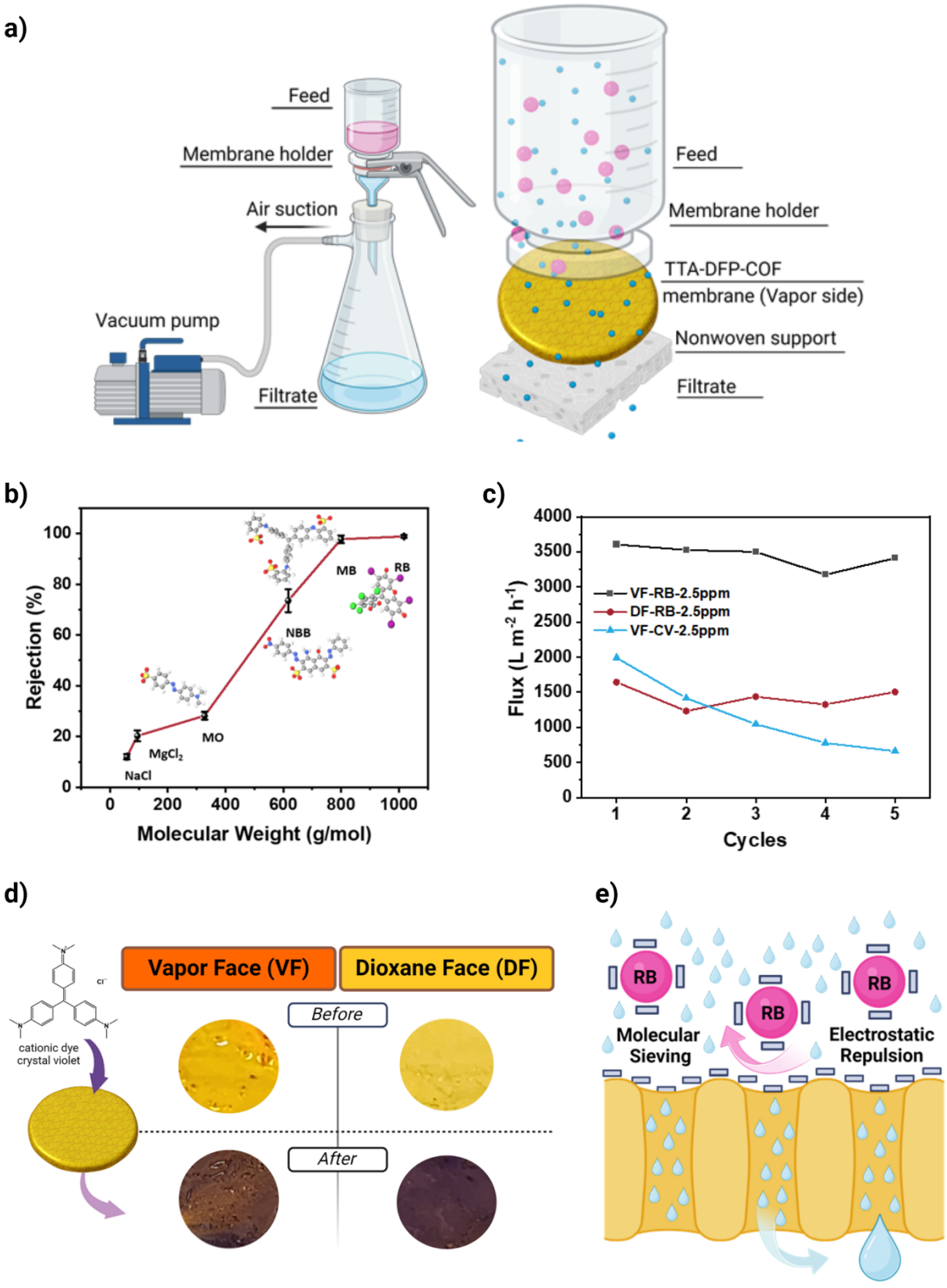

Figure 6. Filtration tests through the TTA-DFP-COF membrane.

a) The filtration assembly, showcasing the vacuum filtration system employed. This system includes a membrane holder comprised of two main parts: the upper section, featuring a cup to contain the feed solution and a support structure to secure the membrane, and the lower section, designed to accommodate the membrane itself, highlighting the specific area where the membrane is positioned.

b) Rejection of salts (NaCl and $MgCl_2$, 1000 mg/L) and dyes (Rose Bengal RB, Methyl Blue MB, Naphthol Blue Black NBB, Methyl Orange MO, 2.5 mg/L) with respect to their molecular weight by TTA-DFP-COF membrane.

c) Variation in water flux through the membrane observed over five cycles, with each cycle processing 10 mL of solution. The assessment involved measuring the water flux for a 2.5 mg/L RB solution filtered through both the VF and DF faces of the membrane, and for a Crystal Violet (CV) solution filtered through the VF face of the membrane.

d) Photographs of the membrane's VF and DF surfaces before and after the 5 cycles of filtration of Crystal Violet (CV), showing the color change caused by CV adsorption on the membrane surface.

e) Proposed mechanism for the rejection of anionic dyes, with RB as an example. The scheme highlights the role of molecular sieving and electrostatic repulsion in the rejection of RB.

Efficient molecular sieving effects

Water contamination by organic micropollutants, including dyes, pharmaceuticals, nano-plastics, and pesticides, presents a significant risk to human health and the environment, attributed to their mutagenic and carcinogenic characteristics.[59] Membrane technologies emerge as a superior alternative for their efficient separation at mild temperatures, despite facing challenges in selectivity, permeability, and fouling.[60,61] Conventional polymeric membranes, in particular, fall short in applications requiring precise molecular sieving, such as the textile industry, which demands effective separation and recovery of toxic effluents.[62,63]

Therefore, we studied the use of TTA-DFP-COF membrane for its high-water flux, superior dye rejection, and enhanced salt permeation capabilities to demonstrate its effectiveness in addressing these challenges. In order to assess the molecular weight cut-off of the synthesized TTA-DFP-COF membrane, four anionic dyes with varying molecular weights and dimensions (Rose Bengal RB, Methyl Blue MB, Naphthol Blue Black NBB, Methyl Orange MO), along with two salts (NaCl and $MgCl_2$), were used as pollutants to assess the membrane's rejection performance (Table S8).

Upon placing the TTA-DFP-COF membrane securely in the filter holder on top of non-woven support, the dye and salt solutions were introduced into the filter holder cup (Figure 6a). For all filtration experiments, the membrane's superhydrophilic vapor face, serving as the active layer, was oriented towards the feed solution. This face was selected for its superior wettability, which enhances the water filtration rate, and its greater negative charge, which boosts dye rejection via electrostatic repulsion with anionic dyes. A vacuum pump was used to facilitate the passage of the feed solution through the membrane.

The outcomes of the filtration tests are presented in Figure 6b, demonstrating the TTA-DFP-COF self-standing membrane's exceptional performance. Consistent with its calculated pore size, the membrane effectively achieved near-total rejection of larger dyes, including Rose Bengal (RB; 11.2 × 12.4 Å) and Methyl Blue (MB, 21.3 × 16.8 Å). In contrast, smaller dyes like Naphthol Blue Black (NBB, 14.6 × 7.9 Å) and Methyl Orange (MO, 12.1 × 2.4 Å) were partially rejected from the dye solutions (2.5 mg/L), highlighting the membrane's selective filtration capability.

To evaluate the membrane's efficacy in rejecting Rose Bengal (RB) at elevated concentrations, a solution containing 20 mg/L RB was tested, resulting in a consistent rejection rate of

approximately 75 %. This indicates the membrane's proficiency in handling high dye concentrations, which is pertinent to the demands of industrial wastewater treatment scenarios.

Using the self-standing TTA-DFP-COF membrane, salt rejection was observed at 12 % for NaCl and 20 % for MgCl2, indicating effective salt permeability. These findings highlight the TTA-DFP-COF membrane's promising capabilities in selective dye/salt separation processes.[64]

Numerous factors could influence the filtration performance of a membrane, including the aperture size of the membrane, the solute size, the membrane surface charge, the solute-solvent interaction, and the solute-membrane interaction. In aquatic solutions, the dyes studied are anionic (RB, MB, NBB, MO). Thus, depending on the membrane's surface charge, the dye's charge might have affected their rejection. To gain deeper insights, we analyzed the ζ-potential results conducted on the membrane vapor and dioxane faces in the context of dye rejection. Since the hydrophilic vapor face used for filtration is negatively charged (-28 mV), as shown in Figure S35, electrostatic repulsion could have played a role in the rejection of the negatively charged dyes. However, all the studied dyes were anionic, yet only the dyes with larger molecular dimensions, specifically RB and MB, achieved complete rejection. Moreover, the molecular sizes of the dye molecules, along with their short-end kinetic diameters, are illustrated in Figure 6b and Table S8, and the membrane pore size calculated for the COF self-standing membrane was around 10.2 Å. Interestingly, the RB dye molecule with a long-end kinetic diameter of 12.4 Å was fully rejected, while the smaller dye molecules and salts were partially able to pass through the pores of the membrane. This suggests that size-sieving and shape-selective mechanisms significantly influenced the filtration process compared to electrostatic repulsion. NBB and RB dyes possess identical charge densities (-2, Table S8), but their size and molecular weight differ significantly. The membrane's higher rejection efficiency for RB than NBB reaffirms its size-selective nature. However, this does not prove that the COF structure’s pores were the main water filtration channels but that the pore size of the membrane filtration channels was in the order of the calculated pore size, allowing the removal of pollutants with bigger sizes.

Furthermore, the negatively charged nature of these dyes suggests that they are more likely to be rejected than adsorbed on the negatively charged membrane surface. Indeed, when the TTA-DFP-COF membrane was immersed in a positively charged dye solution (Rhodamine B) for few minutes, the dioxane face of the membrane displayed the dye's coloration, while the vapor face

retained its characteristic yellow color (Movie 7). Additionally, filtration tests were performed using another cationic dye, crystal violet (CV), with a molecular size (14 × 14 Å) higher than RB (11.2 × 12.4 Å), and the results are shown in Figure 6c. Interestingly, the water filtration rate was quickly decreasing with time until it got to around 660 L m^{-2} h^{-1} after filtering 50 mL, compared to 1990 L m^{-2} h^{-1} at the beginning of the test. After assessing the membrane following the filtration tests, a clear color change is observed on both sides of the membrane, as shown in Figure 6d, indicating that the cationic dye is being adsorbed by the membrane. This is expected given the negatively charged surfaces of the membrane. However, during the anionic dye filtration experiments using RB, no coloring was observed on either face of the membrane, nor a significant drop in the water filtration rate (Figure 6c). This observation signifies that the membrane does not adsorb anionic dyes during filtration tests and further emphasizes the role of the vapor face in rejecting dyes through electrostatic repulsion.

Furthermore, we evaluate the water flow rate through the near-hydrophobic (DF) face of the membrane. Notably, while the DF face demonstrated a similar rejection rate for Rose Bengal (RB) due to its negatively charged surface (−10 mV), it exhibited a lower water permeability, averaging 1428 L m^{-2} h^{-1}, in contrast to the 3443 L m^{-2} h^{-1} observed with the superhydrophilic (VF) face (Figure 6c). Despite this, the performance greatly exceeds that of traditional polymeric membranes.[8] This high water flux suggests that the near-hydrophobic DF face does not hinder water transport, affirming the exceptional capabilities of the TTA-DFP COF self-standing membranes, which offer flux rates significantly higher than conventional options. The remarkable water flux of the TTA-DFP COF membrane is attributed not only to its surface wettability but also to its porosity and the open, interconnected porous structure that enhances flow. In comparison, conventional polymeric membranes, typically used in nanofiltration and reverse osmosis, have water contact angles between 40 and 80° and a denser structure, resulting in lower flux rates.[8] The efficiency of the DF face, thus, stems from the membrane's unique porous architecture and near-hydrophobic surface, promoting superior water flow.

The filtration mechanism for anionic dyes, as illustrated in Figure 6e, employs molecular sieving and electrostatic repulsion to effectively reject RB. This process involves two key strategies: molecular sieving, which permits the passage of water while filtering out larger anionic dye molecules due to the superhydrophilic surface's selective size permeability, and electrostatic

repulsion, where the membrane's negatively charged surface repels anionic dye molecules, preventing their adherence or penetration. Together, these mechanisms facilitate the efficient separation of dyes from water, ensuring thorough dye removal.

Water Purification from Mineral Oil

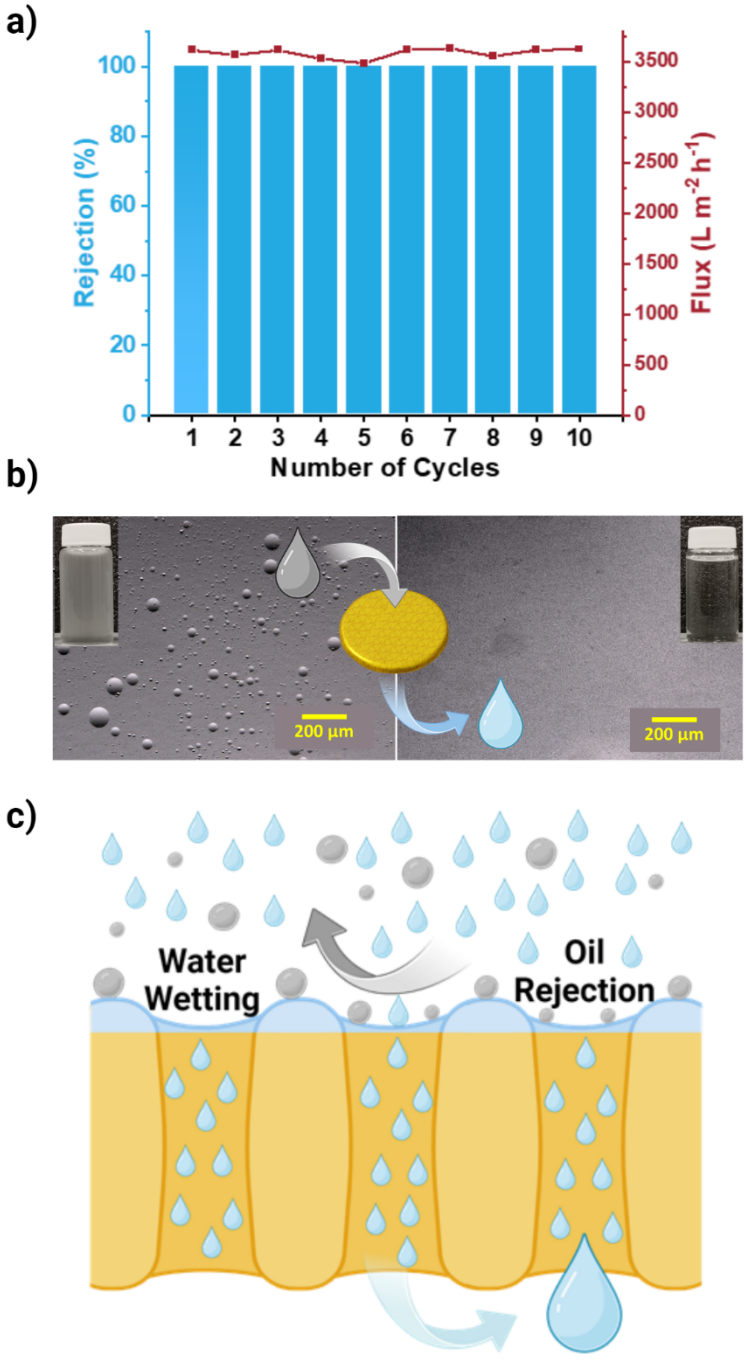

Figure 7. Water Purification from Mineral Oil through the TTA-DFP-COF membrane.

a) Removal of oil from water by TTA-DFP-COF membrane. Left axis (blue): Rejection of oil (1000 mg/L) from oil-in-water suspension over 10 cycles. 40 mL of permeate was collected in

each cycle. Right axis (red): water flux of the oil-in-water suspension through the membrane over 10 cycles.

b) Microscopic images of the oil-in-water suspension before (left) and after (right) filtration through the TTA-DFP-COF membrane. Photographic images of the suspension before and after filtration are also included as insets in each microscopic image.

c) Proposed mechanism for the rejection of mineral oil facing the superhydrophilic VF of the membrane. The scheme highlights the effect of surface complete wetting by water and how it results in high contact angle with oil droplets, thus rejecting oil.

Mineral oil is widely used as a lubricant in machinery and is a key component in the industrial and transport sectors.[65] Leaks, spills, or improper disposal of mineral oil used in machinery can pollute large water bodies even at minimal concentrations, posing a threat to human health and the environment.[66] This resulted in stringent regulations mandating oil/water separation in industrial facilities to purify their wastewater from oil traces before its discharge.

Leveraging the superhydrophilic vapor face of the TTA-DFP COF membrane, we tested its performance in water purification from mineral oil, and the results are shown in Figure 7a. Remarkably, the TTA-DFP-COF membrane exhibited an excellent 99 % oil rejection from water at a significantly high water flux of around 3500 L/m^2.h. This remarkable performance persisted even after several filtration cycles, with each cycle efficiently processing around 40 mL of the 1000 ppm oil-in-water emulsion to produce pure water. This not only highlights the efficiency of the membrane in water purification from oil, but also shows the robustness of the membrane that maintained its performance throughout the tests performed over 10 cycles.

Microscope images shown in Figure 7b further illustrate the presence of oil droplets within the feed solution at a 200 µm scale, offering a clear contrast to the purity of the water permeate post-filtration through the COF membrane. Images of the feed and permeate water in glass vials depict the transition from a cloudy oil-in-water emulsion to clear purified water post-membrane filtration. In the realm of oil-water separation, the surface wettability of the membrane is a critical determinant. Given the superhydrophilic nature of the membrane's vapor face used as the active layer for the oil-in-water emulsion filtration, the water phase spreads across the membrane vapor face before infiltrating its porous structure.[67] This dynamic leads to a high contact angle of the oil phase on the water-wetted membrane vapor-face, reducing its affinity to the membrane vapor-face and culminating in the rejection of the oil phase. The suggested mechanism of removal of oil from water using the COF membrane is schematically represented in Figure 7c. Table S9 in the SI file shows a comparison of the performance of the TTA-DFP-COF membrane reported in this study with recent reports on polymer membranes and composite polymer membranes in oil rejection from oil-in-water emulsions. The TTA-DFP-COF membrane shows superior performance compared to most membranes tested in recent reports, especially in terms of the permeation flux, which is in the range of 100-1000 L m^2 h^{-1} for most non-modified polymer membranes.[68-72]

Antibacterial Properties and biocompatibility

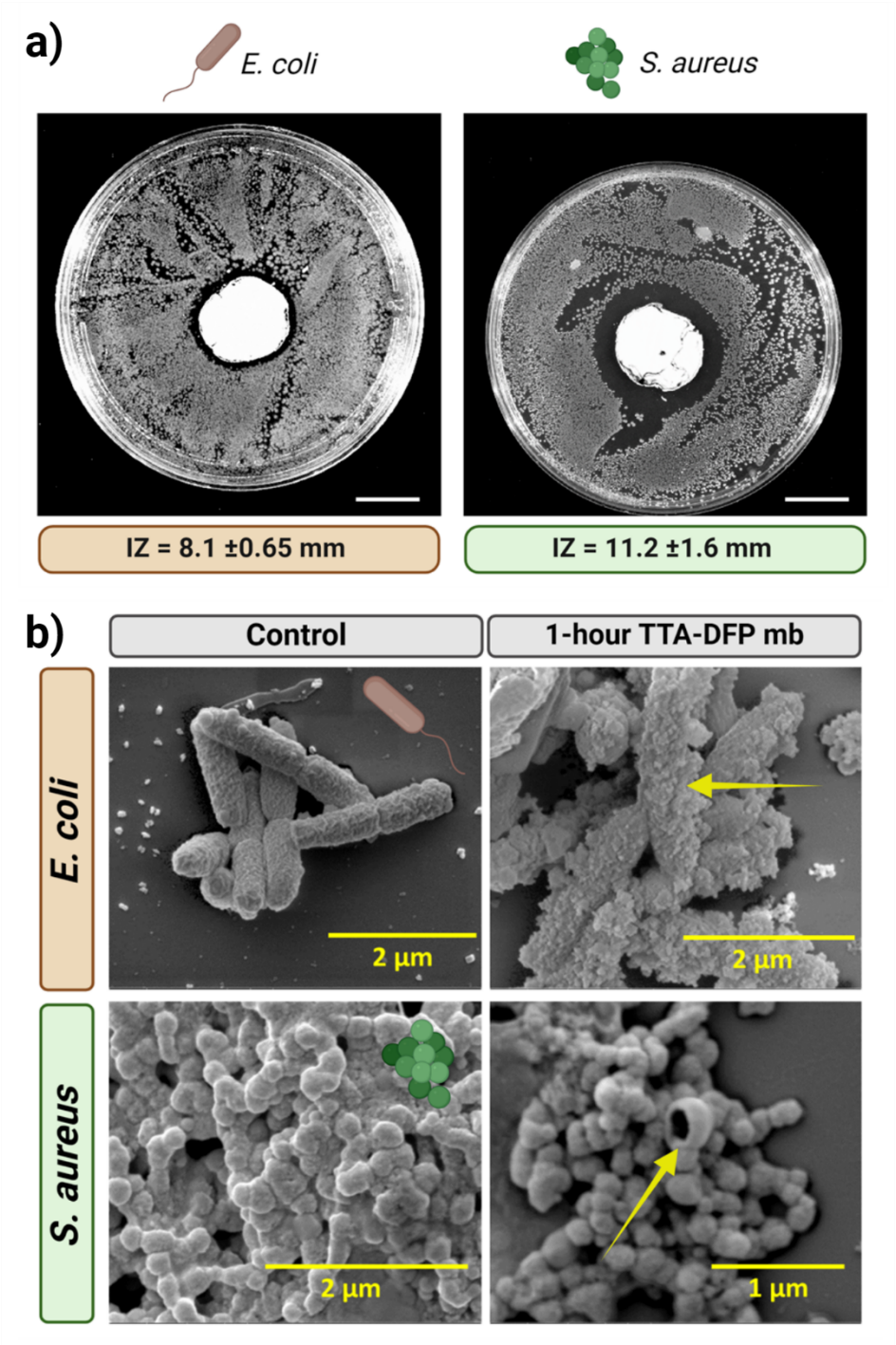

Figure 8. Antimicrobial properties and biocompatibility.

a) Inhibition zone (IZ) images of TTA-DFP-COF membrane against bacteria: *E. coli* as a representative Gram-negative model and *S. aureus* as a typical Gram-positive model.

b) Comparative SEM analysis of bacterial morphology before after 1-hour contact with the TTA-DFP COF membrane. Top panel: *E. coli* bacteria appear intact in control samples but show notable deformation after 1-hour exposure to the TTA-DFP COF membrane, as indicated by the yellow arrows. Bottom panel: *S. aureus* exhibits a similar trend, with control bacteria maintaining their characteristic shape and those treated with the TTA-DFP COF membrane displaying significant structural disruptions, highlighted by yellow arrows.

Advancements in water filtration emphasize the importance of membranes that effectively target both gram-negative and gram-positive bacteria, offering antimicrobial and antibiofouling properties.[73-75] These membranes do more than filter; they protect against various microbes and prevent biofilm formation, enhancing flow rates. Benefits include longer membrane life, reduced maintenance, and clean water supply, essential in healthcare and food industries. Additionally, their broad antimicrobial effectiveness reduces the need for chemicals, leading to greener and more cost-efficient water treatment solutions.

E. coli, representing gram-negative bacteria, and *S. aureus*, representing gram-positive bacteria, were selected to evaluate the membranes' antimicrobial capabilities, including their ability to prevent bacterial attachment and inhibit growth.

The antimicrobial properties of the TTA-DFP-COF membrane (2.5-cm diameter) were first assessed using the agar disc diffusion technique. The zones of inhibition (IZ) surrounding areas treated with TTA-DFP-COF against *E. coli* and *S. aureus* measured 8.1 ±0.65 mm and 11.2 ±1.6 mm in diameter, respectively, after 24 hours of exposure, indicating effective antimicrobial activity (FigureS 8a and S45).

Subsequently, the TTA-DFP COF membrane was exposed to suspensions of *E. coli* and *S. aureus* at a concentration of $1x10^6$ CFU/mL, maintained at 37 °C and agitated for a one-hour period, resulting in antibacterial efficacies of 52.18 % and 80 % respectively, underscoring the membrane's antibacterial properties (Figure S46). Following this exposure, the membrane underwent a washing process and was then incubated in PBS at the same temperature for 4 hours. Agar plate analyses, conducted with samples from both the wash and the eluent bacterial solutions, showed no bacterial presence, confirming the absence of bacterial adherence or survival on the membrane (Figure S47).

The antibacterial efficacy of the TTA-DFP COF membrane against *E. coli* and *S. aureus* was demonstrated by morphological changes observed after 1-hour exposure using SEM. For *E. coli* and *S. aureus*, control cells were intact while those exposed to the membrane showed damage, including holes and blebs leading to potential content leakage and cell death, indicating the membrane's broad-spectrum antibacterial action, as seen in Figures 8b and S48.

The TTA-DFP COF membrane exhibits potent antimicrobial activity, disrupting bacterial cells through electrostatic and hydrogen bond interactions with their membranes. Its efficiency echoes previous findings in triazine and imine-based COFs, which rapidly compromise bacterial membranes, extending antimicrobial effectiveness and preventing biofilm growth.[76-79] The TTA-DFP COF membrane utilizes a contact-killing strategy for antimicrobial defense, providing a sustainable, non-toxic alternative for water treatment that combines environmental safety with effective bacterial control. [80]

The biocompatibility of the TTA-DFP COF membrane was validated *in vitro* with HEK-293 cells, a standard for testing material safety in human biology. After incubating membrane fragments with these cells for 48 hours, optical microscopy showed that cells not only survived but also flourished around and on the membrane, proving its compatibility. This indicates the membrane's safety for use in sensitive environments, ensuring it doesn't compromise water quality.

The TTA-DFP membrane represents an innovative stride in water filtration, combining health, safety, and eco-friendliness. Proven to effectively purify water and combat bacteria while being biocompatible, it stands out as a sustainable choice for meeting global water challenges.

Conclusion

In summary, we developed an innovative approach to rapidly synthesize highly crystalline dual superhydrophilic/near-hydrophobic free-standing COF membranes using a microwave-mediated interfacial polymerization method at the liquid-water vapor interface. This technique achieves COF membranes with exceptional rejection rates, marking it as a breakthrough in COF membrane synthesis. Our method offers a distinct advantage over previous techniques by avoiding the typically slow diffusion and lengthy amorphous-to-crystalline transformation processes. This efficiency directly addresses the existing challenge of preparing COF membranes suitable for molecular separation in a more straightforward manner. Our approach lays the foundation for synthesizing high-quality crystalline free-standing COF membranes.

By tuning the reaction time, we can adjust both the membrane thickness and its wettability characteristics. The TTA-DFP-COF membrane showcases a unique combination of hydrophilic and near-hydrophobic properties derived from its surface chemistry and micro-nanotexture. The smoother vapor face inherits its hydrophilic nature from the reaction between the terminal -NH_2 groups of the TTA precursor and aqueous acetic acid, while the rougher dioxane face is enriched with terminal aldehyde groups.

The duality of this membrane enhances its water permeability, making it superior in resisting organic fouling when compared to standard polymeric membranes. Furthermore, it performs exceptionally in removing oil from oil-in-water mixtures and boasts a water flux of approximately 3600 L/m^2h. This performance is attributed to its multilayered structure and consistent porosity. In tests, the TTA-DFP-COF membranes showed outstanding rejection rates for anionic dyes with sizable molecules, along with significant antimicrobial efficacy against bacteria such as *E. coli* and *S. aureus,* while being biocompatible.

Addressing the scalability issues of our microwave-assisted synthesis for COF membranes, we find our technology particularly suited for small-scale applications. The TTA-DFP-COF membrane sets a new benchmark in membrane technology with its unique properties, making it ideal for use in columnar systems or household water filters. Its simple production, excellent purification performance, and antibacterial properties position it as an innovative solution for tackling the global water crisis, underscoring its importance in providing access to clean water.

Supplemental Information

Document ESI. Supplemental experimental procedures, Figures S1–S37, Tables S1–S9, and supplemental references.

Movie 1: Membrane formation inside microwave, Movie 2: Vapor vs Dioxane Faces, Movie 3: Easy peeling process, Movies 4A, B and C: Membrane formation inside microwave mechanism, Movie 6: mechanical robustness, Movie 7: membrane with Rhodamine.

Acknowledgment

This work was supported by New York University Abu Dhabi and the NYUAD Water Research Center, funded by Tamkeen under the NYUAD Research Institute Award (project CG007), we thank them for their generous support. We thank Sandooq Al Watan (Grant No. SWARD-S22-014, Project ID: PRJ-SWARD-628) and ASPIRE (AARE20-116) for their generous support. The research work was carried out by using the Core Technology Platform resources at NYUAD.

Author contributions

FB and AT conceptualized and oversaw the project's execution. FB spearheaded the membrane synthesis and conducted comprehensive characterizations while AJ executed the water filtration tests. ZM carried out the XPS and AFM experiments. TP was responsible for synthesizing DFP, undertaking PXRD analysis, and handling the computational modeling. HIH, GC, and MER tackled the Raman spectroscopy and ATR-FTIR. SV conducted the solid-state NMR experiments. GD, MA, and BG provided auxiliary support for various characterization tests. MK and ST led the antibacterial assessments, whereas SKS and RJ investigated the membrane's mechanical properties. RGA conducted the BET measurements. JA took charge of measuring surface zeta potential. JW assisted in acquiring SEM images. RP contributed to the TEM study. FG helped analyze the data, especially PXRD. FB, AT, and AJ analyzed the data and wrote the article. All authors discussed the results and revised the manuscript.

Conflicts of interest

There are no conflicts to declare.

References

1. Werber, J.R., Osuji, C.O., and Elimelech, M. (2016). Materials for next-generation desalination and water purification membranes. Nature Reviews Materials *1*, 16018. 10.1038/natrevmats.2016.18.
2. Liang, B., Wang, H., Shi, X., Shen, B., He, X., Ghazi, Z.A., Khan, N.A., Sin, H., Khattak, A.M., and Li, L. (2018). Microporous membranes comprising conjugated polymers with rigid backbones enable ultrafast organic-solvent nanofiltration. Nature Chemistry *10*, 961-967.
3. Gin, D.L., and Noble, R.D. (2011). Designing the Next Generation of Chemical Separation Membranes. Science *332*, 674-676. doi:10.1126/science.1203771.
4. Koros, W.J., and Zhang, C. (2017). Materials for next-generation molecularly selective synthetic membranes. Nature materials *16*, 289-297.
5. El-Kaderi, H.M., Hunt, J.R., Mendoza-Cortés, J.L., Côté, A.P., Taylor, R.E., O'Keeffe, M., and Yaghi, O.M. (2007). Designed Synthesis of 3D Covalent Organic Frameworks. Science *316*, 268-272. doi:10.1126/science.1139915.
6. Furukawa, H., Cordova, K.E., O'Keeffe, M., and Yaghi, O.M. (2013). The chemistry and applications of metal-organic frameworks. Science *341*, 1230444.
7. Waller, P.J., Gándara, F., and Yaghi, O.M. (2015). Chemistry of Covalent Organic Frameworks. Accounts of Chemical Research *48*, 3053-3063. 10.1021/acs.accounts.5b00369.
8. Jrad, A., Olson, M.A., and Trabolsi, A. (2023). Molecular design of covalent organic frameworks for seawater desalination: A state-of-the-art review. Chem *9*, 1413-1451. https://doi.org/10.1016/j.chempr.2023.04.012.
9. Côté, A.P., Benin, A.I., Ockwig, N.W., O'Keeffe, M., Matzger, A.J., and Yaghi, O.M. (2005). Porous, Crystalline, Covalent Organic Frameworks. Science *310*, 1166-1170. doi:10.1126/science.1120411.
10. Huang, N., Wang, P., and Jiang, D. (2016). Covalent organic frameworks: a materials platform for structural and functional designs. Nature Reviews Materials *1*, 16068. 10.1038/natrevmats.2016.68.
11. Song, Y., Sun, Q., Aguila, B., and Ma, S. (2019). Opportunities of covalent organic frameworks for advanced applications. Advanced Science *6*, 1801410.
12. Furukawa, H., and Yaghi, O.M. (2009). Storage of hydrogen, methane, and carbon dioxide in highly porous covalent organic frameworks for clean energy applications. Journal of the American Chemical Society *131*, 8875-8883.
13. Huang, N., Chen, X., Krishna, R., and Jiang, D. (2015). Two-dimensional covalent organic frameworks for carbon dioxide capture through channel-wall functionalization. Angewandte Chemie *127*, 3029-3033.
14. Garai, B., Shetty, D., Skorjanc, T., Gándara, F., Naleem, N., Varghese, S., Sharma, S.K., Baias, M., Jagannathan, R., Olson, M.A., et al. (2021). Taming the Topology of Calix[4]arene-Based 2D-Covalent Organic Frameworks: Interpenetrated vs Noninterpenetrated Frameworks and Their Selective Removal of Cationic Dyes. Journal of the American Chemical Society *143*, 3407-3415. 10.1021/jacs.0c12125.
15. Xu, F., Xu, H., Chen, X., Wu, D., Wu, Y., Liu, H., Gu, C., Fu, R., and Jiang, D. (2015). Radical covalent organic frameworks: a general strategy to immobilize open-accessible

polyradicals for high-performance capacitive energy storage. Angewandte Chemie *127*, 6918-6922.
16. DeBlase, C.R., Silberstein, K.E., Truong, T.-T., Abruña, H.D., and Dichtel, W.R. (2013). β-Ketoenamine-linked covalent organic frameworks capable of pseudocapacitive energy storage. Journal of the American Chemical Society *135*, 16821-16824.
17. Das, G., Garai, B., Prakasam, T., Benyettou, F., Varghese, S., Sharma, S.K., Gándara, F., Pasricha, R., Baias, M., Jagannathan, R., et al. (2022). Fluorescence turn on amine detection in a cationic covalent organic framework. Nature Communications *13*, 3904. 10.1038/s41467-022-31393-2.
18. Dalapati, S., Jin, S., Gao, J., Xu, Y., Nagai, A., and Jiang, D. (2013). An azine-linked covalent organic framework. Journal of the American Chemical Society *135*, 17310-17313.
19. Benyettou, F., Kaddour, N., Prakasam, T., Das, G., Sharma, S.K., Thomas, S.A., Bekhti-Sari, F., Whelan, J., Alkhalifah, M.A., Khair, M., et al. (2021). In vivo oral insulin delivery via covalent organic frameworks. Chemical Science *12*, 6037-6047. 10.1039/D0SC05328G.
20. Fang, Q., Wang, J., Gu, S., Kaspar, R.B., Zhuang, Z., Zheng, J., Guo, H., Qiu, S., and Yan, Y. (2015). 3D porous crystalline polyimide covalent organic frameworks for drug delivery. Journal of the American chemical society *137*, 8352-8355.
21. Bai, L., Phua, S.Z.F., Lim, W.Q., Jana, A., Luo, Z., Tham, H.P., Zhao, L., Gao, Q., and Zhao, Y. (2016). Nanoscale covalent organic frameworks as smart carriers for drug delivery. Chemical communications *52*, 4128-4131.
22. Benyettou, F., Das, G., Nair, A.R., Prakasam, T., Shinde, D.B., Sharma, S.K., Whelan, J., Lalatonne, Y., Traboulsi, H., Pasricha, R., et al. (2020). Covalent Organic Framework Embedded with Magnetic Nanoparticles for MRI and Chemo-Thermotherapy. Journal of the American Chemical Society *142*, 18782-18794. 10.1021/jacs.0c05381.
23. Das, G., Benyettou, F., Sharama, S.K., Prakasam, T., Gándara, F., de la Peña-O'Shea, V.A., Saleh, N.i., Pasricha, R., Jagannathan, R., Olson, M.A., and Trabolsi, A. (2018). Covalent organic nanosheets for bioimaging. Chemical Science *9*, 8382-8387. 10.1039/C8SC02842G.
24. Lin, S., Diercks, C.S., Zhang, Y.-B., Kornienko, N., Nichols, E.M., Zhao, Y., Paris, A.R., Kim, D., Yang, P., and Yaghi, O.M. (2015). Covalent organic frameworks comprising cobalt porphyrins for catalytic CO2 reduction in water. Science *349*, 1208-1213.
25. Vyas, V.S., Haase, F., Stegbauer, L., Savasci, G., Podjaski, F., Ochsenfeld, C., and Lotsch, B.V. (2015). A tunable azine covalent organic framework platform for visible light-induced hydrogen generation. Nature communications *6*, 1-9.
26. Yuan, S., Li, X., Zhu, J., Zhang, G., Van Puyvelde, P., and Van der Bruggen, B. (2019). Covalent organic frameworks for membrane separation. Chemical Society Reviews *48*, 2665-2681. 10.1039/C8CS00919H.
27. Zhang, S., Zhao, S., Jing, X., Niu, Z., and Feng, X. (2021). Covalent organic framework-based membranes for liquid separation. Organic Chemistry Frontiers *8*, 3943-3967. 10.1039/D0QO01354D.
28. Fang, M., Montoro, C., and Semsarilar, M. (2020). Metal and Covalent Organic Frameworks for Membrane Applications. Membranes *10*, 107.

29. Li, J., Zhou, X., Wang, J., and Li, X. (2019). Two-Dimensional Covalent Organic Frameworks (COFs) for Membrane Separation: a Mini Review. Industrial & Engineering Chemistry Research *58*, 15394-15406. 10.1021/acs.iecr.9b02708.
30. Zhang, C., Wu, B.-H., Ma, M.-Q., Wang, Z., and Xu, Z.-K. (2019). Ultrathin metal/covalent–organic framework membranes towards ultimate separation. Chemical Society Reviews *48*, 3811-3841. 10.1039/C9CS00322C.
31. Dey, K., Pal, M., Rout, K.C., Kunjattu H, S., Das, A., Mukherjee, R., Kharul, U.K., and Banerjee, R. (2017). Selective Molecular Separation by Interfacially Crystallized Covalent Organic Framework Thin Films. Journal of the American Chemical Society *139*, 13083-13091. 10.1021/jacs.7b06640.
32. Shinde, D.B., Sheng, G., Li, X., Ostwal, M., Emwas, A.-H., Huang, K.-W., and Lai, Z. (2018). Crystalline 2D Covalent Organic Framework Membranes for High-Flux Organic Solvent Nanofiltration. Journal of the American Chemical Society *140*, 14342-14349. 10.1021/jacs.8b08788.
33. Dai, W., Shao, F., Szczerbiński, J., McCaffrey, R., Zenobi, R., Jin, Y., Schlüter, A.D., and Zhang, W. (2016). Synthesis of a two-dimensional covalent organic monolayer through dynamic imine chemistry at the air/water Interface. Angewandte Chemie *128*, 221-225.
34. Corcos, A.R., Levato, G.A., Jiang, Z., Evans, A.M., Livingston, A.G., Mariñas, B.J., and Dichtel, W.R. (2019). Reducing the Pore Size of Covalent Organic Frameworks in Thin-Film Composite Membranes Enhances Solute Rejection. ACS Materials Letters *1*, 440-446. 10.1021/acsmaterialslett.9b00272.
35. Shinde, D.B., Cao, L., Wonanke, A.D.D., Li, X., Kumar, S., Liu, X., Hedhili, M.N., Emwas, A.-H., Addicoat, M., Huang, K.-W., and Lai, Z. (2020). Pore engineering of ultrathin covalent organic framework membranes for organic solvent nanofiltration and molecular sieving. Chemical Science *11*, 5434-5440. 10.1039/D0SC01679A.
36. Wang, R., Guo, J., Xue, J., and Wang, H. (2021). Covalent Organic Framework Membranes for Efficient Chemicals Separation. Small Structures *2*, 2100061. https://doi.org/10.1002/sstr.202100061.
37. Zhao, S., Jiang, C., Fan, J., Hong, S., Mei, P., Yao, R., Liu, Y., Zhang, S., Li, H., Zhang, H., et al. (2021). Hydrophilicity gradient in covalent organic frameworks for membrane distillation. Nature Materials *20*, 1551-1558. 10.1038/s41563-021-01052-w.
38. Jiang, Y., Liu, C., Li, Y., and Huang, A. (2019). Stainless-steel-net-supported superhydrophobic COF coating for oil/water separation. Journal of Membrane Science *587*, 117177. https://doi.org/10.1016/j.memsci.2019.117177.
39. Wang, H., Wang, M., Wang, Y., Wang, J., Men, X., Zhang, Z., and Singh, V. (2021). Synergistic effects of COF and GO on high flux oil/water separation performance of superhydrophobic composites. Separation and Purification Technology *276*, 119268. https://doi.org/10.1016/j.seppur.2021.119268.
40. Liang, S., Kang, Y., Tiraferri, A., Giannelis, E.P., Huang, X., and Elimelech, M. (2013). Highly Hydrophilic Polyvinylidene Fluoride (PVDF) Ultrafiltration Membranes via Postfabrication Grafting of Surface-Tailored Silica Nanoparticles. ACS Applied Materials & Interfaces *5*, 6694-6703. 10.1021/am401462e.
41. Xiao, K., Wang, X., Huang, X., Waite, T.D., and Wen, X. (2011). Combined effect of membrane and foulant hydrophobicity and surface charge on adsorptive fouling during

microfiltration. Journal of Membrane Science *373*, 140-151. https://doi.org/10.1016/j.memsci.2011.02.041.
42. Younas, H., Bai, H., Shao, J., Han, Q., Ling, Y., and He, Y. (2017). Super-hydrophilic and fouling resistant PVDF ultrafiltration membranes based on a facile prefabricated surface. Journal of Membrane Science *541*, 529-540. https://doi.org/10.1016/j.memsci.2017.07.035.
43. Mohammed, A.K., Al Khoori, A.A., Addicoat, M.A., Varghese, S., Othman, I., Jaoude, M.A., Polychronopoulou, K., Baias, M., Haija, M.A., and Shetty, D. (2022). Solvent-Influenced Fragmentations in Free-Standing Three-Dimensional Covalent Organic Framework Membranes for Hydrophobicity Switching. Angewandte Chemie International Edition *61*, e202200905. https://doi.org/10.1002/anie.202200905.
44. Benyettou, F., Kaddour, N., Prakasam, T., Das, G., Sharma, S.K., Thomas, S.A., Bekhti-Sari, F., Whelan, J., Alkhalifah, M.A., Khair, M., et al. (2021). In vivo oral insulin delivery via covalent organic frameworks. Chem Sci *12*, 6037-6047. 10.1039/d0sc05328g.
45. Rodríguez-Carrillo, C., Benítez, M., El Haskouri, J., Amorós, P., and Ros-Lis, J.V. (2023). Novel Microwave-Assisted Synthesis of COFs: 2020–2022. Molecules *28*, 3112.
46. Kappe, C.O. (2004). Controlled Microwave Heating in Modern Organic Synthesis. Angewandte Chemie International Edition *43*, 6250-6284. https://doi.org/10.1002/anie.200400655.
47. Boyer, M.I., Quillard, S., Rebourt, E., Louarn, G., Buisson, J.P., Monkman, A., and Lefrant, S. (1998). Vibrational Analysis of Polyaniline: A Model Compound Approach. The Journal of Physical Chemistry B *102*, 7382-7392. 10.1021/jp972652o.
48. Ma, T., Wei, L., Liang, L., Yin, S., Xu, L., Niu, J., Xue, H., Wang, X., Sun, J., Zhang, Y.-B., and Wang, W. (2020). Diverse crystal size effects in covalent organic frameworks. Nature Communications *11*, 6128. 10.1038/s41467-020-19858-8.
49. Yang, H.-C., Hou, J., Chen, V., and Xu, Z.-K. (2016). Janus Membranes: Exploring Duality for Advanced Separation. Angewandte Chemie International Edition *55*, 13398-13407. https://doi.org/10.1002/anie.201601589.
50. Chen, X., Weibel, J.A., and Garimella, S.V. (2015). Exploiting Microscale Roughness on Hierarchical Superhydrophobic Copper Surfaces for Enhanced Dropwise Condensation. Advanced Materials Interfaces *2*, 1400480. https://doi.org/10.1002/admi.201400480.
51. Ubuo, E.E., Udoetok, I.A., Tyowua, A.T., Ekwere, I.O., and Al-Shehri, H.S. (2021). The Direct Cause of Amplified Wettability: Roughness or Surface Chemistry? Journal of Composites Science *5*, 213.
52. Ma, C., Nikiforov, A., Hegemann, D., De Geyter, N., Morent, R., and Ostrikov, K. (2023). Plasma-controlled surface wettability: recent advances and future applications. International Materials Reviews *68*, 82-119. 10.1080/09506608.2022.2047420.
53. Jansen, R.J.J., and van Bekkum, H. (1995). XPS of nitrogen-containing functional groups on activated carbon. Carbon *33*, 1021-1027. https://doi.org/10.1016/0008-6223(95)00030-H.
54. Wenzel, R.N. (1936). RESISTANCE OF SOLID SURFACES TO WETTING BY WATER. Industrial & Engineering Chemistry *28*, 988-994. 10.1021/ie50320a024.

55. Liu, J., Han, G., Zhao, D., Lu, K., Gao, J., and Chung, T.-S. (2020). Self-standing and flexible covalent organic framework (COF) membranes for molecular separation. Science Advances *6*, eabb1110. doi:10.1126/sciadv.abb1110.
56. Han, H., Dai, R., and Wang, Z. (2020). Fabrication of High-Performance Thin-Film Composite Nanofiltration Membrane by Dynamic Calcium-Carboxyl Intra-Bridging during Post-Treatment. Membranes *10*, 137.
57. Shevate, R., and Shaffer, D.L. (2022). Large-Area 2D Covalent Organic Framework Membranes with Tunable Single-Digit Nanopores for Predictable Mass Transport. ACS Nano *16*, 2407-2418. 10.1021/acsnano.1c08804.
58. Kandambeth, S., Shinde, D.B., Panda, M.K., Lukose, B., Heine, T., and Banerjee, R. (2013). Enhancement of Chemical Stability and Crystallinity in Porphyrin-Containing Covalent Organic Frameworks by Intramolecular Hydrogen Bonds. Angewandte Chemie International Edition *52*, 13052-13056. https://doi.org/10.1002/anie.201306775.
59. Schwarzenbach, R.P., Escher, B.I., Fenner, K., Hofstetter, T.B., Johnson, C.A., Von Gunten, U., and Wehrli, B. (2006). The challenge of micropollutants in aquatic systems. Science *313*, 1072-1077.
60. Anis, S.F., Lalia, B.S., Lesimple, A., Hashaikeh, R., and Hilal, N. (2022). Electrically conductive membranes for contemporaneous dye rejection and degradation. Chemical Engineering Journal *428*, 131184. https://doi.org/10.1016/j.cej.2021.131184.
61. Qasim, M., Badrelzaman, M., Darwish, N.N., Darwish, N.A., and Hilal, N. (2019). Reverse osmosis desalination: A state-of-the-art review. Desalination *459*, 59-104. https://doi.org/10.1016/j.desal.2019.02.008.
62. Jiang, M., Ye, K., Deng, J., Lin, J., Ye, W., Zhao, S., and Van der Bruggen, B. (2018). Conventional Ultrafiltration As Effective Strategy for Dye/Salt Fractionation in Textile Wastewater Treatment. Environmental Science & Technology *52*, 10698-10708. 10.1021/acs.est.8b02984.
63. Fan, H., Gu, J., Meng, H., Knebel, A., and Caro, J. (2018). High-flux membranes based on the covalent organic framework COF-LZU1 for selective dye separation by nanofiltration. Angewandte Chemie International Edition *57*, 4083-4087.
64. Thamaraiselvan, C., Michael, N., and Oren, Y. (2018). Selective Separation of Dyes and Brine Recovery from Textile Wastewater by Nanofiltration Membranes. Chemical Engineering & Technology *41*, 185-293. https://doi.org/10.1002/ceat.201700373.
65. Rowe, W.B. (2009). Chapter 8 - Application of Fluids. In Principles of Modern Grinding Technology, W.B. Rowe, ed. (William Andrew Publishing), pp. 113-144. https://doi.org/10.1016/B978-0-8155-2018-4.50014-8.
66. Bart, J.C.J., Gucciardi, E., and Cavallaro, S. (2013). 3 - Lubricants: properties and characteristics. In Biolubricants, J.C.J. Bart, E. Gucciardi, and S. Cavallaro, eds. (Woodhead Publishing), pp. 24-73. https://doi.org/10.1533/9780857096326.24.
67. Zhang, N., Yang, X., Wang, Y., Qi, Y., Zhang, Y., Luo, J., Cui, P., and Jiang, W. (2022). A review on oil/water emulsion separation membrane material. Journal of Environmental Chemical Engineering *10*, 107257. https://doi.org/10.1016/j.jece.2022.107257.
68. Xiong, Z., He, Z., Mahmud, S., Yang, Y., Zhou, L., Hu, C., and Zhao, S. (2020). Simple amphoteric charge strategy to reinforce superhydrophilic polyvinylidene fluoride membrane for highly efficient separation of various surfactant-stabilized oil-in-water emulsions. ACS Applied Materials & Interfaces *12*, 47018-47028.

69. Asad, A., Rastgar, M., Sameoto, D., and Sadrzadeh, M. (2021). Gravity assisted super high flux microfiltration polyamide-imide membranes for oil/water emulsion separation. Journal of Membrane Science *621*, 119019.
70. Zhang, H., Shen, Y., Li, M., Zhu, G., Feng, H., and Li, J. (2019). Egg shell powders-coated membrane for surfactant-stabilized crude oil-in-water emulsions efficient separation. ACS Sustainable Chemistry & Engineering *7*, 10880-10887.
71. Deng, W., Fan, T., and Li, Y. (2021). In situ biomineralization-constructed superhydrophilic and underwater superoleophobic PVDF-TiO2 membranes for superior antifouling separation of oil-in-water emulsions. Journal of Membrane Science *622*, 119030.
72. Faraji, M., Nabavi, S.R., and Salimi-Kenari, H. (2020). Fabrication of a PAN–PA6/PANI membrane using dual spinneret electrospinning followed by in situ polymerization for separation of oil-in-water emulsions. New Journal of Chemistry *44*, 13488-13500.
73. Nasir, A.M., Adam, M.R., Mohamad Kamal, S., Jaafar, J., Othman, M.H.D., Ismail, A.F., Aziz, F., Yusof, N., Bilad, M.R., Mohamud, R., et al. (2022). A review of the potential of conventional and advanced membrane technology in the removal of pathogens from wastewater. Sep Purif Technol *286*, 120454. 10.1016/j.seppur.2022.120454.
74. Wu, Y., Xia, Y., Jing, X., Cai, P., Igalavithana, A.D., Tang, C., Tsang, D.C.W., and Ok, Y.S. (2020). Recent advances in mitigating membrane biofouling using carbon-based materials. Journal of Hazardous Materials *382*, 120976. https://doi.org/10.1016/j.jhazmat.2019.120976.
75. Nematollahi, M.H., Mostafavi, E., and Iravani, S. (2023). Covalent organic frameworks and metal-organic frameworks against pathogenic viruses and antibiotic-resistant bacteria: Diagnostic and therapeutic applications. Journal of Environmental Chemical Engineering *11*, 109652. https://doi.org/10.1016/j.jece.2023.109652.
76. Gendy, E.A., Khodair, A.I., Fahim, A.M., Oyekunle, D.T., and Chen, Z. (2022). Synthesis, characterization, antibacterial activities, molecular docking, and computational investigation of novel imine-linked covalent organic framework. Journal of Molecular Liquids *358*, 119191. https://doi.org/10.1016/j.molliq.2022.119191.
77. de Souza Balbinot, G., Mendes Nobre do Espírito Santo, C., Leitune, V.C.B., Visioli, F., Duarte Soares, R.M., Sauro, S., and Collares, F.M. (2022). Antibacterial Effect of Triazine in Barrier Membranes with Therapeutic Activity for Guided Bone Regeneration. Polymers *14*, 4482.
78. RINALDI, A.C., and Scorciapino, M. (2012). Antimicrobial Peptidomimetics: Reinterpreting Nature to Deliver Innovative Therapeutics. Frontiers in Immunology *3*. 10.3389/fimmu.2012.00171.
79. Zhou, C., Min, J., Liu, Z., Young, A., Deshazer, H., Gao, T., Chang, Y.T., and Kallenbach, N.R. (2008). Synthesis and biological evaluation of novel 1,3,5-triazine derivatives as antimicrobial agents. Bioorganic & medicinal chemistry letters *18*, 1308-1311. 10.1016/j.bmcl.2008.01.031.
80. Fang, Z., Lin, Y., Dong, Z., Xu, W., Qi, Y., Zeng, R., Yuan, J., Song, Z., Zhu, F., Liu, H., et al. (2023). Interfacial synthesis of covalent organic framework composited woods for ultrafast ion conduction. Cell Reports Physical Science *4*, 101477. https://doi.org/10.1016/j.xcrp.2023.101477.